BLOC-1 and BLOC-3 regulate VAMP7 cycling to and from melanosomes via distinct tubular transport carriers

Megan K. Dennis[1,2], Cédric Delevoye[3,4], Amanda Acosta-Ruiz[1,2], Ilse Hurbain[3,4], Maryse Romao[3,4], Geoffrey G. Hesketh[5], Philip S. Goff[6], Elena V. Sviderskaya[6], Dorothy C. Bennett[6], J. Paul Luzio[5], Thierry Galli[7], David J. Owen[5], Graça Raposo[3,4] and Michael S. Marks[1,2,8]

[1]Dept. of Pathology and Laboratory Medicine, Children's Hospital of Philadelphia Research Institute, and [2]Dept. of Pathology and Laboratory Medicine and Dept of Physiology, Perelman School of Medicine, University of Pennsylvania, Philadelphia, PA, USA; [3]Institut Curie, PSL Research University, CNRS, UMR144, Structure and Membrane Compartments, F-75005, Paris, France; [4] Institut Curie, PSL Research University, CNRS, UMR144, Cell and Tissue Imaging Facility (PICT-IBiSA), F-75005, Paris, France; [5]Cambridge Institute for Medical Research, University of Cambridge, Cambridge, UK; [6]Cell Biology & Genetics Research Centre, St. George's , University of London, London, UK; [7]Sorbonne Paris-Cité, Univ. Paris-Diderot, Institut Jacques Monod, CNRS UMR7592, INSERM ERL U950, Membrane Traffic in Health & Disease, Paris, France.

[8]To whom correspondence should be addressed:

Michael S. Marks, Ph.D.
Dept. of Pathology & Laboratory Medicine
Children's Hospital of Philadelphia Research Institute
816G Abramson Research Center
3615 Civic Center Blvd.
Philadelphia, PA 19104
Tel: 215-590-3664
Email: marksm@mail.med.upenn.edu

Running title: VAMP7 into and out of melanosomes

Keywords: SNARE, lysosome-related organelle, melanogenesis, Hermansky-Pudlak syndrome, recycling, endosome,

ABSTRACT

Endomembrane organelle maturation requires cargo delivery via fusion with membrane transport intermediates and recycling of fusion factors to their sites of origin. Melanosomes and other lysosome-related organelles obtain cargoes from early endosomes, but the fusion machinery involved and its recycling pathway are unknown. Here, we show that the v-SNARE VAMP7 mediates fusion of melanosomes with tubular transport carriers that also carry the cargo protein, TYRP1, and that require BLOC-1 for their formation. Using live cell imaging, we identify a pathway for VAMP7 recycling from melanosomes that employs distinct tubular carriers. These carriers also harbor the VAMP7-binding scaffold protein, VARP, and the tissue-restricted Rab GTPase, RAB38. Their formation is dependent on the RAB38 exchange factor, BLOC-3. Our data suggest that VAMP7 mediates fusion of BLOC-1-dependent transport carriers with melanosomes, illuminate SNARE recycling from melanosomes as a critical BLOC-3-dependent step, and likely explain the distinct hypopigmentation phenotypes associated with BLOC-1- and BLOC-3-deficiency.

HIGHLIGHTS

- The vSNARE VAMP7 mediates effective delivery of BLOC-1-dependent cargoes to melanosomes
- VAMP7 is delivered to melanosomes from endosomes in BLOC-1-dependent tubules
- VAMP7 recycles from melanosomes in distinct tubules associated with VARP and RAB38
- The RAB38 GEF, BLOC-3, impacts melanogenesis by activating VAMP7 recycling

eTOC BLURB

v-SNAREs mediate fusion of transport carriers with target compartments, but are recycled for repeated transport steps. Dennis et al. show that two protein complexes that are disabled in variants of the human genetic disease Hermansky-Pudlak syndrome regulate cycling of the v-SNARE VAMP7 to and from melanosomes in melanocytes.

INTRODUCTION

Secretory and endolysosomal organelles mature by the membrane transport-dependent delivery of new cargoes and removal of excess material. Cargo delivery requires sorting from a source compartment into nascent transport carriers, transport carrier release and motility towards the target organelle, and tethering, docking and fusion of transport carriers with the maturing target (Bonifacino and Glick, 2004). Cargo removal exploits similar processes, and is particularly important to recycle fusion machinery components to the source membrane for additional rounds of cargo delivery (Bonifacino and Glick, 2004; Jahn and Scheller, 2006). While molecular details underlying fusion machinery cycling among early secretory pathway organelles are well developed (Barlowe and Miller, 2013; Cai et al., 2007), fusion machinery trafficking in the endosomal system is poorly characterized. Proper cycling of fusion machinery is particularly critical during the maturation of lysosome related organelles (LROs), which comprise a class of specialized cell type-specific organelles that derive from the endosomal system but support distinct physiological functions in metazoans (Marks et al., 2013). LRO biogenesis requires dedicated and non-redundant pathways for content delivery; a similar dedicated pathway for content removal has not been described.

The importance of such dedicated pathways in LRO biogenesis is underscored by the defects in patients with Hermansky-Pudlak syndrome (HPS), a group of genetic diseases in which selected LROs fail to mature properly with consequently impaired vision, skin and hair pigmentation, blood clotting and often lung function (Wei and Li, 2013; Wei, 2006). HPS results from mutations in any of at least 10 genes that encode

subunits of four cytoplasmic multisubunit protein complexes: adaptor protein-3 (AP-3) and biogenesis of lysosome-related organelles complex (BLOC)-1, -2 and -3 (Dell'Angelica, 2004; Di Pietro and Dell'Angelica, 2005). These complexes are thought to regulate membrane trafficking during LRO biogenesis, as best characterized in the maturation of melanosomes – the LROs in which melanins are synthesized and stored in pigment cells of the hair, skin and eyes (Sitaram and Marks, 2012). AP-3, BLOC-1 and BLOC-2 effect the delivery of melanogenic enzymes, transporters and accessory proteins from early endosomes to non-pigmented melanosome precursors via two pathways. One pathway requires BLOC-1 (Cullinane et al., 2011; Setty et al., 2008; Setty et al., 2007; Sitaram et al., 2012), in cooperation with the microtubule motor KIF13A and actin remodeling factors (Delevoye et al., 2016; Delevoye et al., 2009), for most analyzed melanosome cargoes to exit endosomes into tubular transport carriers. BLOC-2 then helps target these carriers specifically to melanosomes (Dennis et al., 2015). A second BLOC-1- and BLOC-2-independent pathway requires AP-3 for cargo sorting into melanosome-bound vesicles (Huizing et al., 2001; Setty et al., 2008; Setty et al., 2007; Theos et al., 2005), although AP-3 can also function in the BLOC-1 pathway (Newell-Litwa et al., 2009; Sitaram et al., 2012). How BLOC-3 functions during melanosome biogenesis is not clear. BLOC-3 is a guanine nucleotide exchange factor (GEF) for the cell type-restricted Rab GTPases RAB32 and RAB38 (Gerondopoulos et al., 2012). BLOC-3 and both Rabs are implicated in the biogenesis of melanosomes and other LROs (Bultema et al., 2012; Bultema et al., 2014; Lopes et al., 2007; Osanai et al., 2010; Wasmeier et al., 2006), but whether they function in pathways into or out of melanosomes is not known.

To deliver their contents to maturing melanosomes, endosome-derived transport carriers must fuse with the melanosome membrane. Membrane fusion within the endomembrane system is mediated by SNARE family proteins (Chen and Scheller, 2001; Jahn and Scheller, 2006). Typically, engagement of v-SNAREs (generally R-SNAREs with a central arginine) on the transport carrier with cognate three-helix t-SNARE complexes (generally Qabc SNAREs with central glutamines in the SNARE domains) on the target membrane leads to assembly of stable four-helix bundles that destabilize the membrane and drive fusion (Domanska et al., 2010; Mohrmann et al., 2010). Several SNAREs have been implicated in melanosome biogenesis (Ghiani et al., 2010; Huang et al., 1999; Jani et al., 2015; Tamura et al., 2011; Wade et al., 2001; Yatsu et al., 2013), but among them VAMP7 (a.k.a. tetanus neurotoxin-insensitive or TI-VAMP) is the only v-SNARE. The ubiquitously expressed VAMP7 facilitates fusion of late endosomes with lysosomes (Luzio et al., 2010) and with maturing secretory autophagosomes (Fader et al., 2012; Fader et al., 2009), as well as delivery of GPI-anchored proteins to the plasma membrane (Molino et al., 2015). An additional role for VAMP7 in melanosome maturation is suggested by its localization to melanosomes (Jani et al., 2015) and by the hypopigmentation (Jani et al., 2015) and mistrafficking of the melanosomal protein TYRP1 observed upon VAMP7 depletion (Tamura et al., 2011). Moreover, the VAMP7- and RAB32/38-interacting protein, VARP, is required for proper TYRP1 localization (Tamura et al., 2009) and must bind VAMP7 for this function (Tamura et al., 2011). However, it is not known whether VAMP7 participates directly in fusion of endosome-derived transport carriers with melanosomes, and if so, whether its

function is limited to either the BLOC-1-dependent or –independent pathway. Additionally, although Hrb facilitates VAMP7 recycling from the plasma membrane following fusion with VAMP7-containing organelles such as lysosomes (Pryor et al., 2008), a pathway for recycling of VAMP7 from intracellular organelles to its endosome source in any cell system has not been described.

Here, we exploit quantitative live cell imaging analyses to reveal the dynamics of VAMP7 trafficking in immortalized melanocytes from mouse HPS models. We demonstrate that VAMP7 is a BLOC-1-dependent cargo that most likely functions as the v-SNARE for fusion of the tubular transport intermediates with maturing melanosomes. We also describe a distinct tubular pathway that requires BLOC-3 to recycle VAMP7 from melanosomes following cargo delivery. Our data provide the first evidence of SNARE recycling from a LRO, provide new insights into SNARE recycling within the late endosomal system in mammalian cells, and identify a novel membrane trafficking step in melanocytes that is regulated by BLOC-3.

RESULTS

VAMP7 localizes to melanosomes and is required for melanosome cargo trafficking and pigmentation

VAMP7 has been suggested to localize to melanosomes and to be required for melanogenesis, but its precise function in cargo transport is not known (Jani et al., 2015; Tamura et al., 2011; Yatsu et al., 2013). We first confirmed the localization of VAMP7 in immortal mouse melanocytes derived from C57BL/6 mice [melan-Ink4a or "wild-type" (WT)] (Sviderskaya et al., 2002) and human MNT-1 melanoma cells. When expressed in WT mouse melanocytes, EGFP-tagged VAMP7 (GFP-VAMP7) localized by fluorescence microscopy (FM) extensively to pigmented melanosomes in the cell periphery (82 ± 6%; n=13 cells), and marked pigment granules more predictably ($p<0.0001$) than the melanosomal cargo protein TYRP1 (65 ± 12% overlap; n=13 cells) with which VAMP7 partially overlapped (**Figure 1a-c**). Immunoelectron microscopy (IEM) using immunogold labeling on ultrathin cryosections of transfected melan-a cells confirmed localization of EGFP-VAMP7 to the limiting membrane of pigmented melanosomes and adjacent vesicular structures (**Figure 1d, arrows**). To evaluate the requirement for VAMP7 in cargo trafficking and identify the specific cargo trafficking defect in VAMP7-deficient cells, we depleted VAMP7 in human MNT-1 melanoma cells by siRNA-mediated knockdown (**Figure 1e**). Consistent with previous observations by bright field microscopy (Jani et al., 2015; Yatsu et al., 2013), analysis by standard electron microscopy showed that VAMP7-depleted MNT-1 cells harbored fewer fully pigmented Stage IV melanosomes relative to control siRNA-treated MNT-1 cells (**Figure 1f-g**) and decreased pigmentation (**Figure 1h**). Quantification of immunogold

labeling by IEM showed that whereas TYRP1 localizes predominantly to melanosomes in control siRNA-treated MNT-1 cells, a large cohort is mislocalized to tubulovesicular endosomes adjacent to melanosomes in VAMP7-depleted cells (**Figure 1i-k, arrowheads**). These data support a role for VAMP7 in trafficking melanosomal cargoes such as TYRP1 from endosomes to maturing melanosomes and hence in pigmentation.

VAMP7 traffics to melanosomes in BLOC-1-dependent tubular carriers

To determine whether VAMP7 traffics to melanosomes via BLOC-1-independent or -dependent pathways, we analyzed the localization of GFP-VAMP7 expressed in BLOC-1-deficient (BLOC-$1^{-/-}$) melanocytes relative to melanosomal cargoes and the pan-early endosomal SNARE syntaxin 13 (STX13; a.k.a. syntaxin 12) by FM. In melanocyte cell lines (melan-pa and melan-mu) from two different BLOC-$1^{-/-}$ mouse models (*pallid* and *muted*), GFP-VAMP7 is nearly entirely retained (79 ± 7% in melan-pa; n=53 cells) in sorting and recycling endosomes marked by expression of mCherry-STX13 (mCh-STX13), along with known BLOC-1-dependent cargoes such as TYRP1 (Setty et al., 2007) (**Figure 2a-e** and **Suppl. Figure S1f-i**, arrowheads; compare to WT in **Suppl. Figure 1a-e**, arrows); in fact, the degree to which VAMP7 overlaps with STX13 in these cells is higher ($p<0.0001$) than that of TYRP1 with STX13 [66 ± 14% in melan-pa (Setty et al., 2007)]. Moreover, melanosomal localization of GFP-VAMP7 was restored by stable expression of the missing Pallidin or Muted subunits (melan-pa:MycPa or BLOC-1^{R}, melan-muted:muHA rescue) prior to GFP-VAMP7 expression (**Figure 2f-j; Suppl. Figure 1j-m**). The mislocalization of VAMP7 observed in BLOC-$1^{-/-}$ cells does not reflect global VAMP mistrafficking, as localization of VAMP2, VAMP4 and VAMP8 is

unaffected in BLOC-1^{-} cells compared to WT melanocytes (**Suppl. Figure S2a-f**). Together, these data suggest that VAMP7 is a BLOC-1-dependent cargo protein.

To test whether VAMP7 is targeted to melanosomes in BLOC-1-dependent tubular carriers, we exploited the endosomal retention of VAMP7 in BLOC-1$^{-/-}$ cells. BLOC-1-dependent cargo trafficking in real time is difficult to study in WT melanocytes, as cargoes such as TYRP1 are localized largely to mature pigmented melanosomes at steady state (Orlow et al., 1993; Setty et al., 2007; Vijayasaradhi et al., 1995). Thus, the fraction of TYRP1 undergoing active trafficking to melanosomes is small and difficult to detect. Since stable re-expression of Pallidin in BLOC-1$^{-/-}$ melan-pa melanocytes restores GFP-VAMP7 localization to melanosomes, we surmised that analysis of melan-pa cells soon after transient expression of Pallidin might allow us to visualize early BLOC-1-dependent transport events. To test this, we cotransfected melan-pa cells with myc-Pallidin, GFP-VAMP7 and mCh-STX13 and analyzed fixed cells by FM at various times after transfection. The results (**Figure 2k**-**p**) showed a time-dependent decrease in the extensive overlap between GFP-VAMP7 and mCh-STX13 in endosomes (arrowheads), associated with a concomitant increase in GFP-VAMP7-labeled structures that lacked mCh-STX13 and that likely represent newly forming melanosomes (arrows). The redistribution of GFP-VAMP7 required BLOC-1 function, as it was not observed upon co-transfection of Pallidin-deficient melan-pa cells with an excess of the Muted subunit (**Figures 2k**, **o**, **p** and **S2 g-j**), which does not restore BLOC-1 expression (Setty et al., 2007). The identity of the newly generated GFP-VAMP7-containing, mCh-STX13-negative structures as maturing melanosomes that

had not yet accumulated pigment was supported by their content of TYRP1 (**Suppl. Figure S2k-n**, arrows) and the early stage melanosome marker PMEL (**Suppl. Figure S2s-z**, arrows).

BLOC-1-dependent cargoes such as TYRP1 are transferred from early endosomes to melanosomes via recycling endosomal tubules (Delevoye et al., 2009) that require BLOC-1 for their formation (Delevoye et al., 2016). These transport intermediates and the endosomes from which they derive – but not melanosomes themselves - are labeled by GFP- or mCh-STX13 (Delevoye et al., 2009; Dennis et al., 2015; Setty et al., 2007). To test whether VAMP7 is transported through such carriers, we analyzed melan-pa melanocytes 18 h after co-transfection with myc-Pallidin, GFP-VAMP7 and mCh-STX13. In such transiently rescued BLOC-$1^{-/-}$ cells, unlike in WT or stably rescued BLOC-1^{R} cells in which mCh-STX13 is largely segregated from GFP-VAMP7 and TYRP1-GFP (**Figure 3a-f; Suppl. Movie 1**), tubules emerging from mCh-STX13-labeled endosomes that contain both mCh-STX13 and GFP-VAMP7 (**Figure 3g-j, arrows**) or both mCh-STX13 and TYRP1-GFP (**Figure 3k-n, arrows**) were readily visualized. By contrast, in control mock rescued cells expressing the unrelated Muted BLOC-1 subunit, GFP-VAMP7 was retained in mCh-STX13-positive vacuolar endosomes and was not observed in tubules (**Suppl. Figure S3c-f**, arrowheads). These data provide direct evidence that both melanosomal cargoes and VAMP7 traffic from early endosomes to melanosomes via recycling endosomal tubules. Given the requirement for VAMP7 in optimal transfer of TYRP1 to melanosomes (**Figure 1**), we conclude that VAMP7 likely

functions in fusion of BLOC-1-dependent endosomal carriers with maturing melanosomes.

VAMP7 recycles from melanosomes in tubular carriers that lack STX13

If VAMP7 functions as a canonical v-SNARE in the fusion of vesicular endosomal transport intermediates with maturing melanosomes, it must be retrieved from melanosomes for use in future rounds of cargo delivery. Consistently, we observe GFP-VAMP7-labeled structures emanating from pigmented melanosomes by live cell fluorescence/ bright field microscopy of WT melanocytes (**Figures 4a-c**, **S4a** and **Suppl. Movie 2**). The GFP-VAMP7 labeled tubules (arrows) are distinct from STX13-labeled tubules (arrowheads) that mediate cargo delivery to melanosomes, as assessed using dual-color imaging of WT melanocytes expressing GFP-VAMP7 and mCh-STX13 (**Figure 4d-g** and **Suppl. Movie 1**). This subpopulation of GFP-VAMP7-positive, melanosome-derived tubules are independent of, and shorter in length and less stable than, those labeled solely by mCh-STX13. The GFP-VAMP7 tubules that exit melanosomes do not contain detectable mRFP-tagged OCA2 or TYRP1 (**Figures 4h-j, S4b-f**), suggesting that they are selective for cargo destined for removal from melanosomes. Thus, GFP-VAMP7 labels a population of membrane transport carriers from maturing melanosomes with characteristics consistent with those predicted to be involved in recycling of SNARE proteins and other trafficking machinery (Bonifacino and Glick, 2004; Jahn and Scheller, 2006).

VARP is associated with VAMP7 recycling tubules and is recruited to melanosomes by RAB38 and VAMP7

VAMP7 contains a Longin domain that functions in an autoinhibitory manner to impede VAMP7 interactions with other SNAREs (Martinez-Arca et al., 2003). The scaffolding protein VARP binds both the Longin and SNARE domains of VAMP7 (Burgo et al., 2009), keeping VAMP7 in the autoinhibited conformation and impeding its fusogenic activity (Schäfer et al., 2012). VARP is proposed to support melanosome biogenesis via its ability to bind to VAMP7 (Tamura et al., 2009) and to mediate VAMP7 endosomal recycling in non-LRO-containing cells (Hesketh et al., 2014). Thus, we tested whether VARP associates with VAMP7 recycling from melanosomes. When expressed in WT melanocytes, GFP- or HA- tagged VARP localizes in part (30% ± 6%) to small puncta adjacent to melanosomes in the cell periphery (**Figure 5a-f**), and in part (70% ± 6%) to endosomal structures – as observed in non-melanocytic cells (Hesketh et al., 2014) – that predominate in the perinuclear region (**Figure 5g-i**). By spinning disk microscopy analysis of WT melanocytes coexpressing VARP-GFP and mCh-VAMP7, VARP-GFP is detected on nearly all mCH-VAMP7 tubulovesicular structures (arrows) that exit from melanosomes (arrowhead) in the cell periphery (**Figure 5j-l**, **Suppl. Figure S5a** and **Suppl. Movie 3**). As seen for VAMP7-labeled tubules, VARP-GFP-labeled tubules are not enriched for the melanosomal cargoes TYRP-mRFP or mRFP-OCA2 (**Figures 5m-o**, **S5b, e-h** and **Suppl. Movie 4**). These results place VARP on the VAMP7 recycling tubules exiting melanosomes, where VARP binding would stabilize VAMP7 in a non-fusogenic state during recycling. VARP-GFP-labeled tubules also extend from mCh-STX13-labeled endosomes in the perinuclear region (**Figure 5p-r**, **Suppl. Figure S5c**

and **Suppl. Movie 5**), but are distinct from the STX13-labeled tubules that traffic cargo to melanosomes (**Figure 5s-u** and **Suppl. Figure S5d**), and likely represent carriers that recycle cargoes such as GLUT-1 to the cell surface (Hesketh et al., 2014) or that mediate retrograde endosome to TGN trafficking (Wassmer et al., 2009).

In addition to VAMP7, VARP binds to RAB32/ RAB38 and the VPS29/35 subunits of the retromer complex via distinct binding sites (Burgo et al., 2009; Hesketh et al., 2014; McGough et al., 2014; Tamura et al., 2009; Wang et al., 2008; Zhang et al., 2006) and functions as a RAB21 GEF (Zhang et al., 2006). In non-melanocytic cells, retromer binding is required to recruit VARP to endosome-derived tubules, and both retromer and VARP participate in GLUT-1 trafficking to the cell surface (Hesketh et al., 2014; McGough et al., 2014). In melanocytes, RAB21 GEF activity is dispensable for VARP function, but the interactions with VAMP7 and RAB32/38 are required for proper TYRP1 localization (Tamura et al., 2011), as is retromer (McGough et al., 2014). Like VAMP7, RAB38 and RAB32 localize at least in part to melanosomes (Bultema et al., 2012; Gerondopoulos et al., 2012; Wasmeier et al., 2006) (and **Figure 6a-h**), and thus might function in VARP recruitment. Therefore, we investigated the requirement for VAMP7, RAB32/38, and retromer in recruiting VARP to melanosomes by exploiting defined VARP site-directed mutants in which binding to each partner is impaired (Hesketh et al., 2014). We expressed full-length VARP-GFP or site-directed mutants in WT melanocytes and quantified GFP-positive puncta that associated with pigmented melanosomes (arrowheads) or with mCh-STX13-labeled early endosomes (arrows) (**Figure 6i-o**). Mutagenesis of either VAMP7 or RAB32/38 binding site resulted in

decreased VARP localization to melanosomes by 57%±18% or 60%±19%, respectively, and loss of both binding sites led to a further reduction (87%±11% less than WT). However, consistent with data in non-pigmented cells (Hesketh et al., 2014), these mutations had no effect on the association of VARP with mCh-STX13-labeled early endosomes. In contrast, mutagenesis of the retromer binding site had no effect on melanosome localization but severely impaired association of VARP with mCh-STX13 endosomes as previously observed in non-melanocytic cells (Hesketh et al., 2014). Consistent with a role for RAB38 in recruiting VARP to melanosomes, GFP-RAB38 was enriched at melanosomal puncta that overlapped with VARP-HA in cotransfected cells (**Figure 6a-d**) and mCh-RAB38 was also observed on GFP-VAMP7-containing tubules that exit melanosomes (**Suppl. Figure S5i-l** and **Suppl. Movie 6**). These results indicate that VARP recruitment to pigmented melanosomes is primarily dependent on interactions with both VAMP7 and RAB32/38 and does not require retromer, and that RAB38 accompanies VARP and VAMP7 in retrograde transport carriers.

BLOC-3 is required for RAB38 and VARP recruitment to melanosomes and for the formation of VAMP7 recycling tubules

Although RAB32 and RAB38 have been implicated in melanosome biogenesis (Bultema et al., 2012; Gerondopoulos et al., 2012; Loftus et al., 2002; Wasmeier et al., 2006), whether they function in delivering or exporting cargoes to or from melanosomes is not known. BLOC-3 – composed of HPS1 and HPS4 subunits encoded by the genes that are most frequently targeted by mutations among HPS patients (Seward and Gahl, 2013) – is a RAB32/ RAB38 GEF (Gerondopoulos et al., 2012), but the effects of

BLOC-3 mutations on melanosome biogenesis are also unclear and vary in different pigment cell types (Gardner et al., 1997; Gerondopoulos et al., 2012; Nguyen et al., 2002; Nguyen and Wei, 2007; Richmond et al., 2005). Consistent with the phenotype of BLOC-3-deficient hair bulb melanocytes (Nguyen et al., 2002) and primary mouse melanocyte cultures (Gardner et al., 1997), immortal BLOC-3-deficient melan-le (from HPS4-deficient *light ear* mice) and melan-ep (from (HPS1-deficient *pale ear* mice) melanocytes harbor pigmented melanosomes throughout the cytoplasm, some of which are unusually large (**Figure 7d, m; Suppl. Figures S6g, k, s, w** and **S7c, k, o, w**). The extent of TYRP1 localization to pigment granules in these cells was only slightly reduced from that of WT melanocytes (**Figures 7c-e, Suppl. Figure S6a-p;** 66 ± 6% of TYRP1 overlapped with pigment granules in WT melan-a cells, 56 ± 8% in melan-le; difference is not statistically significant); similarly, segregation of the lysosomal membrane protein LAMP2 from pigment granules was only slightly impaired (**Suppl. Figure S6 a-p;** 5 ± 3% of LAMP2 overlapped with pigment granules in WT melan-a cells, 14 ± 5% in melan-le; $p = 0.003$). These data indicate that BLOC-3 is not directly responsible for anterograde cargo trafficking to melanosomes or for melanosome segregation from the endolysosomal system. Given that GFP-RAB38 associates with VAMP7 recycling tubules, we tested whether RAB38 and VARP localization and VAMP7 recycling were affected by BLOC-3-deficiency. Consistent with BLOC-3 function as a RAB38 GEF, GFP-RAB38 in HPS4-deficient melan-le cells was largely diffuse and did not associate with pigment granules (**Figure 7a-e**). Accordingly, the localization of VARP to melanosomes was also substantially reduced in melan-le cells (**Figure 7k-n**). Stable re-expression of a wild-type HPS4 subunit in HPS4-deficient melan-le

melanocytes, but not of excess wild-type HPS1, restored both RAB38 and VARP melanosomal localization to wild-type levels (**Figure 7f-j; o-r** and **Suppl. Figure S6q-x**). Similar data were obtained using HPS1-deficient melan-ep melanocytes and stable re-expression of HPS1 or HPS4 (**Suppl. Figure 7a-x**). These data indicate that BLOC-3 activation of RAB38 is required for the recruitment and or stabilization of RAB38 on/to melanosomes and for subsequent effective VARP recruitment.

To test whether BLOC-3 is required for VAMP7 recycling, we used live cell imaging to quantify the fission of GFP-VAMP7-containing tubules from melanosomes in transiently transfected WT melanocytes, HPS4-deficient melan-le (le), or melan-le cells stably expressing either HPS1 (le:HPS1) or HPS4 (le:HPS4). As in WT melanocytes, the majority of GFP-VAMP7 (78 ± 9%, n=23 cells; not significantly different from WT) localized to melanosomes in the periphery of melan-le cells (**Fig. 7b**). However, whereas recycling tubules were frequently observed emanating from these structures in WT cells (**Figure 7s, v; Suppl. Movie 7**), such tubules were much rarer in melan-le cells (**Figure 7t, v**). Restoration of BLOC-3 function by stable expression of HPS4 restored WT tubule frequency, whereas stable expression of HPS1 did not (**Figure 7u, v**). These data indicate that BLOC-3 regulates recycling of VAMP7 from melanosomes, most likely by recruiting RAB38 and consequently VARP to initiate and/or complete tubule formation.

DISCUSSION

VAMP7 has been implicated in melanosome biogenesis (Jani et al., 2015; Tamura et al., 2011), but the pathways by which it is directed toward and recycled from melanosomes were not known. Here we show that VAMP7 functions primarily as a v-SNARE in BLOC-1-dependent tubular transport from endosomes to melanosomes, and thereby promotes melanosomal delivery of BLOC-1-dependent cargoes such as TYRP1. Importantly, our analyses of VAMP7 dynamics revealed a previously undocumented SNARE recycling pathway from maturing melanosomes. This pathway employs membrane tubules that emerge from melanosomes at sites enriched in RAB38 and VARP and that require the RAB32/RAB38 GEF, BLOC-3, for their formation. Our data define a specific membrane transport pathway in which RAB32/RAB38 and BLOC-3 participate, and have important implications for BLOC-3 and VAMP7 function in the biogenesis of other lysosome-related organelles and in the etiology of the most common forms of Hermansky-Pudlak syndrome.

Cargoes are delivered to melanosomes by two distinct pathways that emerge from early endosomes, one that requires BLOC-1 and a second that is BLOC-1-independent (Sitaram and Marks, 2012). Our data using a novel transient rescue assay clearly show that VAMP7 traffics to melanosomes via STX13-containing endosomal tubules that require BLOC-1 for their formation. BLOC-1-dependent melanosomal cargoes such as TYRP1 traverse these same endosomal intermediates, and are largely trapped together with VAMP7 in early endosomes in BLOC-1-deficient cells. That VAMP7 is a cargo of

the BLOC-1 pathway is consistent with observations in BLOC-1-deficient neurons, fibroblasts and 293T cells in which VAMP7 levels in cell extracts (and synaptic vesicle fractions of neurons) were reduced (Ryder et al., 2013; Salazar et al., 2006). Moreover, the altered TYRP1 distribution in cells depleted of VAMP7 indicates that VAMP7 likely functions as the main v-SNARE for cargo delivery in this pathway. Given that STX13 labels the BLOC-1-dependent transport intermediates (Dennis et al., 2015), this function for VAMP7 likely explains the reported requirement for VAMP7 in the accumulation of a truncated form of STX13 on melanosomes (Jani et al., 2015). VAMP7 might similarly function in fusion of tubular intermediates observed between endosomes and lysosomes in cell types that lack LROs (Bright et al., 2005); such tubules might be generated through the action of BLOC-1, which is required for the formation of a subclass of recycling endosomes (Delevoye et al., 2016), or perhaps by the structurally related BORC (Pu et al., 2015).

All v-SNARE proteins are thought to cycle back to their membrane of origin following cargo delivery in order to mediate additional rounds of cargo trafficking (Bonifacino and Glick, 2004; Jahn and Scheller, 2006). However, in mammalian cells, other than the Hrb-dependent recycling of VAMP7 from the plasma membrane following fusion with late endosomes (Pryor et al., 2008), pathways for v-SNARE recycling in the late endosomal system have not been described. Here, we visualized the recycling of VAMP7 from melanosomes in small tubular intermediates that also contain VARP and RAB38. Melanosomal cargoes were not enriched in these tubules, indicating that the tubules are cargo-selective. The association of these tubules with VARP, which

maintains VAMP7 in an inactive form (Schäfer et al., 2012), implies that the VAMP7 within them is inactive, as expected for a recycling v-SNARE; VARP may be released prior to fusion with the target organelle, allowing VAMP7 to serve as a vSNARE on the recycling step. It is not clear how cargo is selected for entry into the tubules, but AP-3 - which engages VAMP7 on early endosomes (Kent et al., 2012; Martinez-Arca et al., 2003) and has recently been suggested to facilitate STX13 recycling from melanosomes (Jani et al., 2015) – is unlikely to participate in this process since VAMP7 is localized normally in AP-3-deficient melanocytes (unpublished data). However, the dramatic depletion of VAMP7-containing recycling tubules in cells lacking BLOC-3 suggests that RAB38 and/or RAB32 play an important role in recruiting effectors for cargo selection, tubule formation and/or tubule release. RAB38 and RAB32 have been shown to engage Myosin Vc (Bultema et al., 2014); it is possible that this myosin might primarily facilitate recycling tubule dynamics with secondary effects on melanosome secretion (Bultema et al., 2014). Through their recruitment of VARP, RAB38 and VAMP7 might indirectly participate in the recruitment of other recycling effectors, akin to the recruitment of the kinesin-1 motor KIF5 by VARP in neurons (Burgo et al., 2012). Given that BLOC-3 is expressed ubiquitously (Chiang et al., 2003; Martina et al., 2003; Nazarian et al., 2003), we speculate that it may facilitate VAMP7 recycling from other organelles in cell types that lack LROs, perhaps through activation of very low levels of RAB32 or RAB38 or of a distinct RAB GTPase. While we were unable to define the target organelle for these rapidly motile tubules by single plane spinning disc microscopy, we speculate that they ultimately return VAMP7 to STX13-containing early endosomes either directly or via an intermediate compartment such as late endosomes or the plasma membrane. Note that

although binding to retromer was not required for VARP recruitment to melanosomes, our data do not negate a role for retromer in either anterograde or retrograde transport as recently proposed (McGough et al., 2014).

While the biochemical role of BLOC-3 as a GEF for RAB32 and RAB38 is well-established (Gerondopoulos et al., 2012), the physiological roles of BLOC-3 and its target RABs during melanosome biogenesis were unclear. Simultaneous depletion of RAB32 and RAB38 (Bultema et al., 2012; Loftus et al., 2002; Wasmeier et al., 2006) or VARP (Tamura et al., 2011; Tamura et al., 2009) in skin melanocytes results in pigment dilution and TYR and TYRP1 mislocalization largely to the Golgi and/or TGN. Similarly, retinal pigment epithelia (RPE) from RAB38-deficient *chocolate* mice are depleted of melanosomes and mislocalize a cohort of TYR (Lopes et al., 2007), and depletion of either RAB32, RAB38 or BLOC-3 subunits in MNT-1 melanoma cells causes loss of pigmentation (Gerondopoulos et al., 2012). Although these data suggested a direct role in anterograde traffic, they could also be explained by an indirect role through a failure of VAMP7 recycling and its resulting entrapment on melanosomes; this would lead to depletion of VAMP7 from the endosomal source of melanosome cargoes and a consequent secondary failure in anterograde trafficking similar to that observed upon VAMP7 depletion [refs. (Jani et al., 2015; Tamura et al., 2011) and **Figure 1**]. This model for a primary role in retrograde transport would be consistent with the localization of RAB32 and RAB38 primarily to melanosomes [refs. (Bultema et al., 2012; Gerondopoulos et al., 2012) and **Figure 6a-h**] and secondarily to tubulovesicular membranes that were speculated to be anterograde transport intermediates but might

reflect retrograde tubules (Wasmeier et al., 2006). RAB38 and RAB32 have also been reported to interact with AP-1, BLOC-1 and BLOC-2, all on the anterograde pathway to melanosomes (Bultema et al., 2012); these interactions might serve as a mechanism to coordinate anterograde and retrograde trafficking.

Intriguingly, a primary role for BLOC-3 and RAB32/RAB38 in VAMP7 recycling could also explain the variable phenotypes of pigmented cells in BLOC-3-deficient mice (Gardner et al., 1997; Nguyen and Wei, 2007) and HPS patients (Anderson et al., 2003; Takeuchi et al., 2014). In eyes of BLOC-3-deficient *light ear* or *pale ear* mice, retinal pigment epithelia are hypopigmented, with numerous small, lightly pigmented melanosomes, whereas cells of the adjacent choroid contain highly pigmented macromelanosomes (Gardner et al., 1997; Suzuki et al., 2002). Similarly, melanocytes in the hair bulb are pigmented with enlarged but otherwise normal melanosomes (Nguyen et al., 2002), as in the immortalized melan-ep and melan-le melanocytes used here, whereas in the interfollicular melanocytes of the skin – as in BLOC-3-depleted MNT-1 cells (Gerondopoulos et al., 2012) and primary melanocytes of HPS1 patients (Boissy et al., 1998) – the few detectable melanosomes are small and hypopigmented (Nguyen and Wei, 2007); these differences result in dark fur and hypopigmented skin (Lane and Green, 1967). We speculate that these cell type-specific differences in melanosome biogenesis reflect different requirements for VAMP7 recycling in maintaining an endosomal pool of VAMP7 for anterograde transport. For example, cell types with low levels of VAMP7 expression and/or high rates of melanosome biogenesis would deplete VAMP7 from endosomes and hence block anterograde cargo trafficking

required for melanosome biogenesis, resulting in fewer, smaller and hypopigmented melanosomes. Alternatively, cell types with high levels of VAMP7 expression and/or low rates of melanosome biogenesis might restore sufficient levels of endosomal VAMP7 biosynthetically to compensate for the loss of recycling and permit sufficient anterograde cargo delivery for new melanosome synthesis. The enlarged melanosomes in such cells would result from (1) continued anterograde membrane delivery without compensating retrograde membrane retrieval and (2) fusion of melanosomes with each other and with other organelles due to an excess of "unprotected" fusogenically uninhibited VAMP7 lacking VARP. A similar rationale might explain the differences in melanosome biogenesis in the RPE and choroidal melanocytes in RAB38-deficient *chocolate* mice (Brooks et al., 2007; Lopes et al., 2007), and perhaps the defect in TYRP1 localization in VARP-depleted melan-a cells (Tamura et al., 2011; Tamura et al., 2009). While future analyses of the rates of melanosome biogenesis and VAMP7 biosynthesis will be necessary to test the validity of these models, the identification of a VAMP7 recycling pathway from melanosomes that is regulated by BLOC-3 provides a new way of thinking about an old problem.

EXPERIMENTAL PROCEDURES

Reagents

Chemicals were obtained from Sigma-Aldrich, except where noted. Hygromycin B was from Roche. Tissue culture reagents and Lipofectamine 2000 were from Invitrogen. Matrigel was from Becton Dickinson.

Cell culture and generation of stable cells

Immortalized melanocyte cell lines melan-Ink4a-1 (a.k.a. melan-Ink-4a-Arf-1; referred to here as melan-Ink4a or WT) derived from C57BL/6 *Ink4a-Arf*$^{-/-}$ mice (Sviderskaya et al., 2002), melan-ep1 (referred to here as melan-ep) derived from BLOC-3-deficient C57BL/6J *Hps1*$^{ep/ep}$ *pale ear* mice and melan-le1 (referred to here as melan-le) derived from BLOC-3-deficient C57BL/6J *Hps4*$^{le/le}$ *light ear* mice (Chiang et al., 2003; Suzuki et al., 2002), and melan-pa1 (referred to here as melan-pa) derived from BLOC-1 deficient C57BL/6J-*Pldn*$^{pa/pa}$ *pallid* mice, melan-mu1 (referred to here as melan-mu) derived from BLOC-1 deficient B6.CHMU/Le *Muted*$^{mu/mu}$ *muted* mice and stably transduced melan-pa:myc-Pa and melan-mu:MuHA lines in which BLOC-1 function is restored via expression of the missing subunit (Setty et al., 2007) have been described. All cells were cultured in RPMI 1640 medium supplemented with 10% FBS (Atlanta Biologicals) and 200 nM 12-*O*-tetradecanoylphorbol-13-acetate (TPA). Melan-le, melan-ep and stable lines derived from these cells were also cultured in the presence of 200 pM cholera toxin. Stably transduced cell lines were generated by infection with recombinant retroviruses produced in transiently transfected Plat-E cells (Morita et al., 2000) and selection with 100 μg/ml (for melan-ep based lines) or 150 μg/ml (for melan-le based

lines) hygromycin B as described (Meng et al., 2012; Setty et al., 2007). Stable cell lines were occasionally treated with hygromycin B (100 or 150 µg/ml) to maintain selection for transgene expression. In most experiments, cells were transiently transfected with expression plasmids using Lipofectamine 2000 (1 µl with 800 ng DNA, including carrier DNA as needed, in 100 µl Opti-MEM for each coverslip in a 24 well plate or 4 µl Lipofectamine 2000 with 4 µg DNA in 500 µl Opti-MEM for 35 mm glass-bottom dishes) and imaged at varying times following transfection as indicated. Only cells with low or modest levels of transgene expression were chosen for analysis, and DNA amounts were titrated to ensure modest but detectable expression in 10-40% of transfected cells.

Antibodies

The following monoclonal antibodies were used: mouse anti-TYRP1 (TA99) was from ATCC; rat anti-LAMP1 (1D4B) and rat anti-LAMP2 (GL2A7) were from Developmental Studies Hybridoma Bank; mouse anti-PMEL (HMB-45) was from Lab Vision; and mouse anti-HA.11 was from Covance. Anti-VAMP7 mAb (158.2) and pAb (TG50) have previously been described and validated using *Vamp7*$^{-/-}$ mice (Danglot et al., 2012). Polyclonal rabbit antisera to STX13 (Prekeris et al., 1998) has been previously described and rabbit anti-giantin was from Abcam (ab24586). Species-specific secondary antibodies from donkey conjugated to Alexa Fluor 488, 594 or 647 or Dylite 488, 594 or 647 used in IFM were from Jackson ImmunoResearch Laboratories.

DNA constructs and siRNAs

The siRNAs used were: human VAMP7 siRNA, 5′-CTGCCAAGACAGGATTGTATA-3′ (Danglot et al., 2010); control siRNA 5’-AATTCTCCGAACGTGTCACGT-3’. Recombinant retroviral vectors pBMN-X/N-IRES-Hygro-HA3-hHPS1 and pBMN-X/N-IRES-Hygro-HA3-hHPS4 encoding human HPS1 and HPS4 under the control of the Maloney murine leukemia virus (MMLV) promoter were generated by subcloning the XhoI-NotI cDNA fragment from pCI-HA3-humanHPS1 and pCI-HA3-humanHPS4 (gifts from J. Bonifacino; National Institutes of Health, Bethesda, MD) into pBMN-X/N-IRES-Hygro. pCR3-mRFP-OCA2, pmCh-C1-STX13, pEGFP-C1-STX13, pEGFP-N1-TYRP-EGFP (Dennis et al., 2015); pBMN-IRES-Hygro-mycPa, pBMN-IRES-Hygro-mycMu (Setty et al., 2007); pLXIN-huVARP-HA2 (Schäfer et al., 2012); pLXIN-huVARP-EGFP, pLXIN-huVARP(M684D, Y687S)-EGFP, pLXIN, huVARP(Q509A,Y550A)-EGFP, pLXIN-huVARP(H432S,L434A,H712S,L714A)-EGFP, pEGFP-N1-VARP(WT)-EGFP (Hesketh et al., 2014) have been previously described. pmRFP-N1-TYRP-mRFP was generated by amplifying mRFP from pmRFP-N1 by PCR and subcloning the resulting SalI-NotI fragment into pEGFP-N1-huTYRP1. pEGFP-C2-RAB38 was a gift from A. Hume (University of Nottingham). mCh-RAB38 controlled by the CMV promoter was generated by subcloning mCh into pEGFP-C2-RAB38 using the AgeI-XhoI region of mCh from pmCh-C1 (Takara Bio Inc.). pLXIN-VAMP4-HA (Gordon et al., 2009) was a gift from A. Peden (University of Sheffield). EGFP-VAMP2, EGFP-VAMP7 and EGFP-VAMP8 in pEGFP-C vector, controlled by the CMV promoter and generated from mouse cDNA, were gifts from P. Roche (National Institutes of Health, Bethesda, MD). pmCh-VAMP7 controlled by the CMV promoter was generated by subcloning mCh into pEGFP-C-VAMP7 using the AgeI-BsrGI region of mCh from pmCh-C1 (Takara Bio Inc.).

Electron microscopy

For conventional EM, MNT-1 cells were fixed with 2.5% glutaraldehyde in 0.1 M cacodylate buffer (1.5 h on ice), post-fixed with 1% OsO_4/ 1.5% potassium ferricyanide (45 min on ice), dehydrated in ethanol and embedded in Epon resin. For ultrathin cryosectioning, MNT-1 cells fixed with 2% PFA and 0.2% glutaraldehyde in 0.1 M phosphate buffer (pH 7.4) were processed for ultracryomicrotomy and immunogold labeled using TYRP1 antibody (TA99) followed by protein A conjugated to 10 nm gold (PAG10). Electron micrographs were acquired using Philips CM120 or Tecnai Spirit G2 (FEI, Eindhoven, The Netherlands) equipped with a numeric camera (Keen View; Soft Imaging System) or 4k CCD camera (Quemesa, Olympus, Muenster, Germany).

Immunoblotting

MNT-1 cells were seeded at 1 x 10^6 per 10 cm Petri dish and transfected with Oligofectamine (Invitrogen) 2 days later with control- or VAMP7-specific siRNAs and then again after an additional 3 days. Three days after, cells were washed in cold PBS and incubated in cold lysis buffer (50 mM Tris, 150 mM NaCl, 0.1 % Triton X-100, 10 mM EDTA, pH 7.2 supplemented with protease inhibitor cocktail [Roche]) for 20 min on ice. Cell lysates were collected by scraping and clarified by centrifugation for 15 min at 13,000 rpm (4°C). Lysates were incubated with sample buffer (2x concentrated), boiled for 5 min and processed for immunoblotting.

Quantification of melanin content

MNT-1 cells were seeded at 1 x 10^5 per well in a 6-well plate and transfected twice with siRNA as for immunoblotting. Three days after the second siRNA transfection, cells were washed twice in cold PBS and incubated with 200 µl of cold melanin buffer (50 mM Tris, 150 mM NaCl, 2 mM EDTA, pH 7.2). Cells were scraped, sonicated and 100 µl of lysate was centrifuged at 13,000 rpm for 15 minutes at 4 °C. Supernatants were removed and pellets washed with 500 µl of Ethanol/Ether (1:1 ratio) and dissolved in 230 µl of 2 M NaOH/ 20% DMSO for 1 h at 60 °C. The optical density at 490 nm of 200 µl of solubilized melanin was measured and normalized to protein content evaluated by Bradford assay (Thermo Scientific).

Fluorescence microscopy

Standard IFM and colocalization analyses

Cells were plated on Matrigel-coated coverslips, fixed with 3% paraformaldehyde (PFA) in Hanks buffered salt solution (HBSS), labeled with primary and secondary antibodies and mounted using Vectashield H-1000 (Vector Labs). Cells were analyzed by epifluorescence microscopy on a Leica DM IRBE or DMI 6000B microscope equipped with a 63× Plan Apochromat objective (1.4 NA) and either a Retiga EXi Fast 1394 or a Hamamatsu ORCA-Flash4.0 sCMOS digital camera. Images were acquired in z-stacks using a 0.2 µm step size and deconvolved using either subtractive volume deconvolution with OpenLab (PerkinElmer) software or Gold's Method deconvolution with three iterations in LASX (Leica) software. Quantification of the area of overlap in the cell periphery between two fluorescent labels or a fluorescent label and pigmented

melanosomes was carried out using ImageJ (http://fiji.sc/Fiji; National Institutes of Health) on wide-field fluorescence images using a method similar to that previously used with OpenLab software (Setty et al., 2007). In brief, images were cropped to contain a single cell with the nucleus and perinuclear area removed, and binary images of fluorescence were generated by subtracting the local background before thresholding using parameters of a rolling ball radius of 10 pixels with smoothing disabled. Binary images of pigment granules from bright-field imaging were generated by manual thresholding. The Image Calculator function was used to generate an image representing the area of overlap between channels by multiplying the binary images for each of the two channels. The areas of overlap and of total fluorescent labeling in structures larger than 5 pixels were quantified using the Analyze Particles function; the ratio of overlap pixels to total fluorescent pixels in the channel of interest gives the percentage of overlap.

Transient rescue of BLOC-1$^-$ cells expressing GFP-VAMP7, TYRP-GFP and mCh-STX13

BLOC-1$^-$ melan-pa cells were seeded on Matrigel-coated coverslips in 24-well tissue culture plates and 24 h later transiently transfected with Lipofectamine using 200 ng each of pEGFP-C-VAMP7 and pmCh-C1-STX13 and 500 ng of either pBMN-IRES-Hygro-mycMu or pBMN-IRES-Hygro-mycPa. At indicated times after transfection, cells were fixed with 3% PFA in HBSS and either mounted directly using Vectashield (Vector Labs) or processed for IFM as described above with either TA99 or HMB-45 and Dylite647-conjugated secondary antibodies. Cells were imaged as for standard IFM.

The number of GFP-VAMP7-positive, mCH-STX13-negative puncta was quantified by manual counting within selected 200 × 200 pixel regions in the periphery of cells. Quantification of overlap between GFP-VAMP7 and mCh-STX13 in the cell periphery was completed as described above for standard IFM colocalization.

Quantification of melanosomal and endosomal VARP localization using site-directed VARP mutants

WT melanocytes were seeded on Matrigel-coated coverslips and transfected using Lipofectamine 2000 with mCH-STX13 and either pLXIN-VARP(WT)-EGFP or the site-directed pLXIN-VARP-GFP mutants deficient for binding to VAMP7 only, RAB38 only, VAMP7 and RAB38, or retromer. 48 h following transfection, cells were fixed and processed for standard IFM and deconvolved using LASX and Gold's Method (three iterations). Quantification of VARP-GFP puncta associated with melanosomes visualized by bright field microscopy or associated with mCh-STX13-labeled endosomes was done by manual counting after excluding a 200 pixel diameter circular selection containing the nucleus and Golgi region.

Live-cell imaging

Cells were seeded in Matrigel-coated 35 mm glass-bottomed dishes and transiently transfected with indicated GFP- or mCh/mRFP- fusion proteins using Lipfectamine 2000. At indicated times following transfection, cells in riboflavin-free RPMI (US Biological) containing 10% FBS were imaged on a Zeiss Axiovert 200 microscope equipped with an UltraVIEW ERS6 spinning disk confocal scan head (Perkin Elmer), an environmental

chamber at 37°C, an Orca ER CCD camera (Hamamatsu) and Volocity (Perkin Elmer) software for image acquisition. In some experiments, an ORCA FLASH 4.0 sCMOS camera was used instead. For imaging of cells expressing GFP-VAMP7 relative to melanosomes imaged by bright field microscopy (Figure 4a-c), we used an Olympus IX71 spinning disk confocal microscope equipped with a LCI Chamlide stagetop incubation chamber at 37°C/ 5% CO_2, an ImageEM EM-CCD camera (Hamamatsu Photonics) and MetaMorph (Molecular Devices) software for image acquisition. Image sequences were further analyzed using ImageJ. All images were captured at ~1 fps except for Supplemental Movie S3, which was captured at ~1.4 fps.

Quantification of GFP-VAMP7 tubules leaving melanosomes

To quantify the number of GFP-VAMP7 tubules leaving melanosomes in WT, BLOC-3-deficient and BLOC-3-rescued cells, cells were seeded on Matrigel-coated glass-bottom plates, transfected with GFP-VAMP7 using Lipofectamine 2000 and imaged 24 h after transfection. Image sequences were acquired for 5 minutes at ~1 fps (300 images) as for other live cell imaging described above. Quantification was completed using ImageJ Fiji. First, the peri-nuclear region of each cell was excluded by placing a circular region of interest (ROI) with diameter 200 pixels over the nucleus and adjacent Golgi region as visualized by an accumulation of GFP-VAMP7 signal. 50 x 50 pixel regions were cropped from the periphery of each cell, avoiding the nuclear ROI and edges of the cell. Local background was subtracted from these 50 px^2 regions using the “Process -> Subtract Background…” command in ImageJ with settings of rolling ball radius of 10 pixels and all other boxes unchecked; the resulting “background subtracted” file was

further processed using the “Smooth” command to yield a “smoothed” file. The “Combine” command was then used to place the “background subtracted” and “smoothed” files adjacent to each other, and only tubules that were observed in both files were included in the quantification. For quantification, the number of GFP-VAMP7 tubules/vesicles observed to depart from GFP-VAMP7-labeled melanosomes was manually counted over all 300 frames of an image sequence.

Statistical analysis

Statistical significance was determined by the unpaired two-tailed Student’s *t* test. All values are indicated as ± SD (n, cells analyzed). *, $P < 0.05$; **, $P < 0.01$; ***, $P < 0.005$; ****, $P < 0.0001$.

AUTHOR CONTRIBUTIONS

MKD, CD, GR and MSM conceived of the project with input from JPL, TG and DJO. MKD, CD, AAR, IH, MR, JGH, PSG and GR performed experiments and with MSM analyzed data. GGH, EVS, DCB, JPL, TG and DJO provided invaluable reagents prior to publication. MKD and MSM drafted and all authors edited the manuscript.

ACKNOWLEDGMENTS

We thank Jan Burkhardt and the Penn Cell and Developmental Biology Microscopy Core (especially Andrea Stout) for the use of spinning disc microscopes, the Nikon Imaging Center @ Institut Curie-CNRS, and the PICT-IBiSA, member of the France-BioImaging national research infrastructure, supported by the CelTisPhyBio Labex (N° ANR-10-LBX-0038) part of the IDEX PSL (N°ANR-10-IDEX-0001-02 PSL), Juan Bonifacino, Alistair Hume, Andrew Peden and Paul Roche for gifts of expression plasmids, and Dawn Harper for technical help. We are grateful for funding from the following sources: National Institutes of Health grants R01 EY015625 (to MSM and GR) from the National Eye Institute, R01 AR048155 (to MSM) and F32 AR062476 (to MKD) from the National Institute of Arthritis, Musculoskeletal and Skin Diseases, R01 GM108807 (to MSM) from the National Institute for General Medical Sciences, Fondation pour la Recherche Médicale (FRM) to TG, the UK Medical Research Council, G0900113 (to JPL), the Wellcome Trust, 108429 (to EVS and DCB), a Canadian Institutes of Health Research Fellowship (GGH), CNRS, INSERM, Institut Curie and Fondation pour la Recherche Médicale (FRM grant DEQ20140329491 Team label to GR).

REFERENCES

Anderson, P.D., Huizing, M., Claassen, D.A., White, J., and Gahl, W.A. (2003). Hermansky-Pudlak syndrome type 4 (HPS-4): clinical and molecular characteristics. Hum Genet *113(1):10-7*, 10-17.

Barlowe, C.K., and Miller, E.A. (2013). Secretory protein biogenesis and traffic in the early secretory pathway. Genetics *193*, 383-410.

Boissy, R.E., Zhao, Y., and Gahl, W.A. (1998). Altered protein localization in melanocytes from Hermansky-Pudlak syndrome: support for the role of the HPS gene product in intracellular trafficking. Lab Invest *78*, 1037-1048.

Bonifacino, J.S., and Glick, B.S. (2004). The mechanisms of vesicle budding and fusion. Cell *116*, 153-166.

Bright, N.A., Gratian, M.J., and Luzio, J.P. (2005). Endocytic delivery to lysosomes mediated by concurrent fusion and kissing events in living cells. Curr Biol *15*, 360-365.

Brooks, B.P., Larson, D.M., Chan, C.C., Kjellstrom, S., Smith, R.S., Crawford, M.A., Lamoreux, L., Huizing, M., Hess, R., Jiao, X.*, et al.* (2007). Analysis of ocular hypopigmentation in Rab38cht/cht mice. Invest Ophthalmol Vis Sci *48*, 3905-3913.

Bultema, J.J., Ambrosio, A.L., Burek, C.L., and Di Pietro, S.M. (2012). BLOC-2, AP-3, and AP-1 function in concert with Rab38 and Rab32 to mediate protein trafficking to lysosome-related organelles. J Biol Chem *287*, 19550-19563.

Bultema, J.J., Boyle, J.A., Malenke, P.B., Martin, F.E., Dell'Angelica, E.C., Cheney, R.E., and Di Pietro, S.M. (2014). Myosin vc interacts with rab32 and rab38 proteins and works in the biogenesis and secretion of melanosomes. J Biol Chem *289*, 33513-33528.

Burgo, A., Proux-Gillardeaux, V., Sotirakis, E., Bun, P., Casano, A., Verraes, A., Liem, R.K., Formstecher, E., Coppey-Moisan, M., and Galli, T. (2012). A molecular network for the transport of the TI-VAMP/VAMP7 vesicles from cell center to periphery. Dev Cell *23*, 166-180.

Burgo, A., Sotirakis, E., Simmler, M.C., Verraes, A., Chamot, C., Simpson, J.C., Lanzetti, L., Proux-Gillardeaux, V., and Galli, T. (2009). Role of Varp, a Rab21 exchange factor and TI-VAMP/VAMP7 partner, in neurite growth. EMBO Rep *10*, 1117-1124.

Cai, H., Reinisch, K., and Ferro-Novick, S. (2007). Coats, tethers, rabs, and SNAREs work together to mediate the intracellular destination of a transport vesicle. Dev Cell *12*, 671-682.

Chen, Y.A., and Scheller, R.H. (2001). SNARE-mediated membrane fusion. Nat Reviews, Mol Cell Biol *2*, 98-106.

Chiang, P.-W., Oiso, N., Gautam, R., Swank, R.T., and Spritz, R.A. (2003). The Hermansky-Pudlak syndrome 1 (HPS1) and HPS4 proteins are components of two complexes, BLOC-3 and BLOC-4, involved in the biogenesis of lysosome-related organelles. J Biol Chem *278*, 20332-20337.

Cullinane, A.R., Curry, J.A., Carmona-Rivera, C., Summers, C.G., Ciccone, C., Cardillo, N.D., Dorward, H., Hess, R.A., White, J.G., Adams, D.*, et al.* (2011). A BLOC-1 mutations screen reveals that *PLDN* is mutated in Hermansky-Pudlak syndrome type 9. Am J Human Genet *88*, 778-787.

Danglot, L., Chaineau, M., Dahan, M., Gendron, M.C., Boggetto, N., Perez, F., and Galli, T. (2010). Role of TI-VAMP and CD82 in EGFR cell-surface dynamics and signaling. Journal of cell science *123*, 723-735.

Danglot, L., Zylbersztejn, K., Petkovic, M., Gauberti, M., Meziane, H., Combe, R., Champy, M.F., Birling, M.C., Pavlovic, G., Bizot, J.C.*, et al.* (2012). Absence of TI-VAMP/Vamp7 leads to increased anxiety in mice. The Journal of neuroscience : the official journal of the Society for Neuroscience *32*, 1962-1968.

Delevoye, C., Heiligenstein, X., Ripoll, L., Gilles-Marsens, F., Dennis, M.K., Linares, R.A., Derman, L., Gokhale, A., Morel, E., Faundez, V.*, et al.* (2016). BLOC-1 Brings Together the Actin and Microtubule Cytoskeletons to Generate Recycling Endosomes. Curr Biol *26*, 1-13.

Delevoye, C., Hurbain, I., Tenza, D., Sibarita, J.-B., Uzan-Gafsou, S., Ohno, H., Geerts, W.J.C., Verkleij, A.J., Salamero, J., Marks, M.S.*, et al.* (2009). AP-1 and KIF13A coordinate endosomal sorting and positioning during melanosome biogenesis. J Cell Biol *187*, 247-264.

Dell'Angelica, E.C. (2004). The building BLOC(k)s of lysosomes and related organelles. Curr Opin Cell Biol *16*, 458–464.

Dennis, M.K., Mantegazza, A.R., Snir, O.L., Tenza, D., Acosta-Ruiz, A., Delevoye, C., Zorger, R., Sitaram, A., de Jesus-Rojas, W., Ravichandran, K.*, et al.* (2015). BLOC-2 targets recycling endosomal tubules to melanosomes for cargo delivery. The Journal of cell biology *209*, 563-577.

Di Pietro, S.M., and Dell'Angelica, E.C. (2005). The cell biology of Hermansky-Pudlak syndrome: recent advances. Traffic *6*, 525-533.

Domanska, M.K., Kiessling, V., and Tamm, L.K. (2010). Docking and fast fusion of synaptobrevin vesicles depends on the lipid compositions of the vesicle and the acceptor SNARE complex-containing target membrane. Biophysical journal *99*, 2936-2946.

Fader, C.M., Aguilera, M.O., and Colombo, M.I. (2012). ATP is released from autophagic vesicles to the extracellular space in a VAMP7-dependent manner. Autophagy *8*, 1741-1756.

Fader, C.M., Sanchez, D.G., Mestre, M.B., and Colombo, M.I. (2009). TI-VAMP/VAMP7 and VAMP3/cellubrevin: two v-SNARE proteins involved in specific steps of the autophagy/multivesicular body pathways. Biochimica et biophysica acta *1793*, 1901-1916.

Gardner, J.M., Wildenberg, S.C., Keiper, N.M., Novak, E.K., Rusiniak, M.E., Swank, R.T., Puri, N., Finger, J.N., Hagiwara, N., Lehman, A.L.*, et al.* (1997). The mouse pale ear (ep) mutation is the homologue of human Hermansky-Pudlak syndrome. Proc Natl Acad Sci USA *94*, 9238-9243.

Gerondopoulos, A., Langemeyer, L., Liang, J.-R., Linford, A., and Barr, F.A. (2012). BLOC-3 mutated in Hermansky-Pudlak syndrome is a Rab32/38 guanine nucleotide exchange factor. Curr Biol *22*, 2135-2139.

Ghiani, C.A., Starcevic, M., Rodriguez-Fernandez, I.A., Nazarian, R., Cheli, V.T., Chan, L.N., Malvar, J.S., de Vellis, J., Sabatti, C., and Dell'angelica, E.C. (2010). The dysbindin-containing complex (BLOC-1) in brain: developmental regulation, interaction with SNARE proteins and role in neurite outgrowth. Mol Psychiatry *15*, 204-215.

Gordon, D.E., Mirza, M., Sahlender, D.A., Jakovleska, J., and Peden, A.A. (2009). Coiled-coil interactions are required for post-Golgi R-SNARE trafficking. EMBO reports *10*, 851-856.

Hesketh, G.G., Pérez-Dorado, I., Jackson, L.P., Wartosch, L., Schäfer, I.B., Gray, S.R., McCoy, A.J., Zeldin, O.B., Garman, E.F., Harbour, M.E.*, et al.* (2014). VARP is recruited on to endosomes by direct interaction with retromer, where together they function in export to the cell surface. Dev Cell *29*, 591-606.

Huang, L., Kuo, Y.M., and Gitschier, J. (1999). The pallid gene encodes a novel, syntaxin 13-interacting protein involved in platelet storage pool deficiency. Nature Genet *23*, 329-332.

Huizing, M., Anikster, Y., Fitzpatrick, D.L., Jeong, A.B., D'Souza, M., Rausche, M., Toro, J.R., Kaiser-Kupfer, M.I., White, J.G., and Gahl, W.A. (2001). Hermansky-Pudlak syndrome type 3 in Ashkenazi Jews and other non-Puerto Rican patients with hypopigmentation and platelet storage-pool deficiency. Am J Hum Genet *69*, 1022-1032.

Jahn, R., and Scheller, R.H. (2006). SNAREs — engines for membrane fusion. Nature Rev Mol Cell Biol *7*, 631-643.

Jani, R.A., Purushothaman, L.K., Rani, S., Bergam, P., and Setty, S.R. (2015). STX13 regulates cargo delivery from recycling endosomes during melanosome biogenesis. Journal of cell science *128*, 3263-3276.

Kent, H.M., Evans, P.R., Schäfer, I.B., Gray, S.R., Sanderson, C.M., Luzio, J.P., Peden, A.A., and Owen, D.J. (2012). Structural basis of the intracellular sorting of the SNARE VAMP7 by the AP3 adaptor complex. Dev Cell *22*, 979-988.

Lane, P.W., and Green, E.L. (1967). Pale ear and light ear in the house mouse. Mimic mutations in linkage groups XII and XVII. The Journal of heredity *58*, 17-20.

Loftus, S.K., Larson, D.M., Baxter, L.L., Antonellis, A., Chen, Y.A., Wu, X.S., Jiang, Y., Bittner, M., Hammer, J.A., III, and Pavan, W.J. (2002). Mutation of melanosome protein RAB38 in chocolate mice. Proc Natl Acad Sci USA *99*, 4471-4476.

Lopes, V.S., Wasmeier, C., Seabra, M.C., and Futter, C.E. (2007). Melanosome maturation defect in Rab38-deficient retinal pigment epithelium results in instability of immature melanosomes during transient melanogenesis. Mol Biol Cell *18*, 3914-3927.

Luzio, J.P., Gray, S.R., and Bright, N.A. (2010). Endosome-lysosome fusion. Biochemical Society transactions *38*, 1413-1416.

Marks, M.S., Heijnen, H.F.G., and Raposo, G. (2013). Lysosome-related organelles: unusual compartments become mainstream. Curr Opin Cell Biol *25*, 495-505.

Martina, J.A., Moriyama, K., and Bonifacino, J.S. (2003). BLOC-3, a protein complex containing the Hermansky-Pudlak syndrome gene products HPS1 and HPS4. J Biol Chem *278*, 29376-29384.

Martinez-Arca, S., Rudge, R., Vacca, M., Raposo, G., Camonis, J., Proux-Gillardeaux, V., Daviet, L., Formstecher, E., Hamburger, A., Filippini, F.*, et al.* (2003). A dual mechanism controlling the localization and function of exocytic v-SNAREs. Proc Natl Acad Sci USA *100*, 9011-9016.

McGough, I.J., Steinberg, F., Gallon, M., Yatsu, A., Ohbayashi, N., Heesom, K.J., Fukuda, M., and Cullen, P.J. (2014). Identification of molecular heterogeneity in SNX27-retromer-mediated endosome-to-plasma-membrane recycling. J Cell Sci *127*, 4940-4953.

Meng, R., Wang, Y., Yao, Y., Zhang, Z., Harper, D.C., Heijnen, H.F.G., Sitaram, A., Li, W., Raposo, G., Weiss, M.J.*, et al.* (2012). SLC35D3 delivery from megakaryocyte early endosomes is required for platelet dense granule biogenesis and differentially defective in Hermansky-Pudlak syndrome models. Blood *120*, 404-414.

Mohrmann, R., de Wit, H., Verhage, M., Neher, E., and Sorensen, J.B. (2010). Fast vesicle fusion in living cells requires at least three SNARE complexes. Science *330*, 502-505.

Molino, D., Nola, S., Lam, S.M., Verraes, A., Proux-Gillardeaux, V., Boncompain, G., Perez, F., Wenk, M., Shui, G., Danglot, L.*, et al.* (2015). Role of tetanus neurotoxin insensitive vesicle-associated membrane protein in membrane domains transport and homeostasis. Cellular logistics *5*, e1025182.

Morita, S., Kojima, T., and Kitamura, T. (2000). Plat-E: an efficient and stable system for transient packaging of retroviruses. Gene Ther *7*, 1063-1066.

Nazarian, R., Falcón-Pérez, J.M., and Dell'Angelica, E.C. (2003). Biogenesis of lysosome-related organelles complex 3 (BLOC-3): A complex containing the Hermansky-Pudlak syndrome (HPS) proteins HPS1 and HPS4. Proc Natl Acad Sci USA *100*, 8770-8775.

Newell-Litwa, K., Salazar, G., Smith, Y., and Faundez, V. (2009). Roles of BLOC-1 and adaptor protein-3 complexes in cargo sorting to synaptic vesicles. Mol Biol Cell *20*, 1441-1453.

Nguyen, T., Novak, E.K., Kermani, M., Fluhr, J., Peters, L.L., Swank, R.T., and Wei, M.L. (2002). Melanosome morphologies in murine models of Hermansky-Pudlak syndrome reflect blocks in organelle development. J Invest Dermatol *119*, 1156-1164.

Nguyen, T., and Wei, M.L. (2007). Hermansky-Pudlak HPS1/pale ear gene regulates epidermal and dermal melanocyte development. J Invest Dermatol *127*, 421-428.

Orlow, S.J., Boissy, R.E., Moran, D.J., and Pifko-Hirst, S. (1993). Subcellular distribution of tyrosinase and tyrosinase-related protein-1: implications for melanosomal biogenesis. J Invest Dermatol *100*, 55-64.

Osanai, K., Higuchi, J., Oikawa, R., Kobayashi, M., Tsuchihara, K., Iguchi, M., Huang, J., Voelker, D.R., and Toga, H. (2010). Altered lung surfactant system in a Rab38-deficient rat model of Hermansky-Pudlak syndrome. Am J Lung Cell Mol Physiol *298*, L243-L251.

Prekeris, R., Klumperman, J., Chen, Y.A., and Scheller, R.H. (1998). Syntaxin 13 mediates cycling of plasma membrane proteins via tubulovesicular recycling endosomes. J Cell Biol *143*, 957-971.

Pryor, P.R., Jackson, L., Gray, S.R., Edeling, M.A., Thompson, A., Sanderson, C.M., Evans, P.R., Owen, D.J., and Luzio, J.P. (2008). Molecular basis for the sorting of the SNARE VAMP7 into endocytic clathrin-coated vesicles by the ArfGAP Hrb. Cell *134*, 817-827.

Pu, J., Schindler, C., Jia, R., Jarnik, M., Backlund, P., and Bonifacino, J.S. (2015). BORC, a multisubunit complex that regulates lysosome positioning. Developmental cell *33*, 176-188.

Richmond, B., Huizing, M., Knapp, J., Koshoffer, A., Zhao, Y., Gahl, W.A., and Boissy, R.E. (2005). Melanocytes derived from patients with HermanskyPudlak Syndrome types 1, 2, and 3 have distinct defects in cargo trafficking. J Invest Dermatol *124*, 420-427.

Ryder, P.V., Vistein, R., Gokhale, A., Seaman, M.N., Puthenveedu, M., and Faundez, V. (2013). The WASH complex, and endosomal Arp2/3 activator, interacts with the Hermansky-Pudlak syndrome complex BLOC-1 and its cargo phosphatidylinositol-4 kinase type II alpha. Mol Biol Cell *24*, 2269-2284.

Salazar, G., Craige, B., Styers, M.L., Newell-Litwa, K.A., Doucette, M.M., Wainer, B.H., Falcon-Perez, J.M., Dell'Angelica, E.C., Peden, A.A., E. Werner, E.*, et al.* (2006). BLOC-1 complex deficiency alters the targeting of Adaptor Protein complex-3 cargoes. Mol Biol Cell *17*, 4014-4026.

Schäfer, I.B., Hesketh, G.G., Bright, N.A., Gray, S.R., Pryor, P.R., Evans, P.R., Luzio, J.P., and Owen, D.J. (2012). The binding of Varp to VAMP7 traps VAMP7 in a closed, fusogenically inactive conformation. Nat Struct Mol Biol *19*, 1300-1309.

Setty, S.R.G., Tenza, D., Sviderskaya, E.V., Bennett, D.C., Raposo, G., and Marks, M.S. (2008). Cell-specific ATP7A transport sustains copper-dependent tyrosinase activity in melanosomes. Nature *454*, 1142-1146.

Setty, S.R.G., Tenza, D., Truschel, S.T., Chou, E., Sviderskaya, E.V., Theos, A.C., Lamoreux, M.L., Di Pietro, S.M., Starcevic, M., Bennett, D.C.*, et al.* (2007). BLOC-1 is required for cargo-specific sorting from vacuolar early endosomes toward lysosome-related organelles. Mol Biol Cell *18*, 768-780.

Seward, S.L., Jr., and Gahl, W.A. (2013). Hermansky-Pudlak syndrome: health care throughout life. Pediatrics *132*, 153-160.

Sitaram, A., Dennis, M.K., Chaudhuri, R., De Jesus-Rojas, W., Tenza, D., Setty, S.R.G., Wood, C.S., Sviderskaya, E.V., Bennett, D.C., Raposo, G.*, et al.* (2012). Differential recognition of a dileucine-based sorting signal by AP-1 and AP-3 reveals a requirement for both BLOC-1 and AP-3 in delivery of OCA2 to melanosomes. Mol Biol Cell *23*, 3178-3192.

Sitaram, A., and Marks, M.S. (2012). Mechanisms of protein delivery to melanosomes in pigment cells. Physiology *27*, 85-99.

Suzuki, T., Li, W., Zhang, Q., Karim, A., Novak, E.K., Sviderskaya, E.V., Hill, S.P., Bennett, D.C., Levin, A.V., Nieuwenhuis, H., K.*, et al.* (2002). Hermansky-Pudlak syndrome is caused by mutations in HPS4, the human homolog of the mouse light-ear gene. Nature Genet *30*, 321-324.

Sviderskaya, E.V., Hill, S.P., Evans-Whipp, T.J., Chin, L., Orlow, S.J., Easty, D.J., Cheong, S.C., Beach, D., DePinho, R.A., and Bennett, D.C. (2002). p16Ink4a in melanocyte senescence and differentiation. J Natl Cancer Inst *94*, 446-454.

Takeuchi, S., Abe, Y., Yamada, T., Kawano, S., Hozumi, Y., Ito, S., Suzuki, T., and Nishigori, C. (2014). Case of Hermansky-Pudlak syndrome 1 patient with milder symptoms in Japanese. The Journal of dermatology *41*, 268-270.

Tamura, K., Ohbayashi, N., Ishibashi, K., and Fukuda, M. (2011). Structure-function analysis of VPS9-ankyrin-repeat protein (Varp) in the trafficking of tyrosinase-related protein 1 in melanocytes. J Biol Chem *286*, 7507-7521.

Tamura, K., Ohbayashi, N., Maruta, Y., Kanno, E., Itoh, T., and Fukuda, M. (2009). Varp is a novel Rab32/38-binding protein that regulates Tyrp1 trafficking in melanocytes. Mol Biol Cell *20*, 2900-2908.

Theos, A.C., Tenza, D., Martina, J.A., Hurbain, I., Peden, A.A., Sviderskaya, E.V., Stewart, A., Robinson, M.S., Bennett, D.C., Cutler, D.F.*, et al.* (2005). Functions of AP-3 and AP-1 in tyrosinase sorting from endosomes to melanosomes. Mol Biol Cell *16*, 5356-5372.

Vijayasaradhi, S., Xu , Y.Q., Bouchard, B., and Houghton, A.N. (1995). Intracellular sorting and targeting of melanosomal membrane proteins: identification of signals for sorting of the human brown locus protein, gp75. J Cell Biol *130*, 807-820.

Wade, N., Bryant, N.J., Connolly, L.M., Simpson, R.J., Luzio, J.P., Piper, R.C., and James, D.E. (2001). Syntaxin 7 complexes with mouse Vps10p tail interactor 1b, Syntaxin 6, vesicle-associated membrane protein (VAMP)8, and VAMP7 in B16 melanoma cells. J Biol Chem *276*, 19820-19827.

Wang, F., Zhang, H., Zhang, X., Wang, Y., Ren, F., Zhang, X., Zhai, Y., and Chang, Z. (2008). Varp interacts with Rab38 and functions as its potential effector. Biochem Biophys Res Commun *372*, 162-167.

Wasmeier, C., Romao, M., Plowright, L., Bennett, D.C., Raposo, G., and Seabra, M.C. (2006). Rab38 an Rab32 control early post-Golgi trafficking of melanogenic enzymes. J Cell Biol *175*, 271-281.

Wassmer, T., Attar, N., Harterink, M., van Weering, J.R., Traer, C.J., Oakley, J., Goud, B., Stephens, D.J., Verkade, P., Korswagen, H.C.*, et al.* (2009). The retromer coat complex coordinates endosomal sorting and dynein-mediated transport, with carrier recognition by the trans-Golgi network. Developmental cell *17*, 110-122.

Wei, A.-H., and Li, W. (2013). Hermansky-Pudlak syndrome: Pigmentary and non-pigmentary defects and their pathogenesis. Pigment Cell Melanoma Res *26*, 176-192.

Wei, M.L. (2006). Hermansky–Pudlak syndrome: a disease of protein trafficking and organelle function. Pigment Cell Res *19*, 19-42.

Yatsu, A., Ohbayashi, N., Tamura, K., and Fukuda, M. (2013). Syntaxin-3 is required for melanosomal localization of Tyrp1 in melanocytes. The Journal of investigative dermatology *133*, 2237-2246.

Zhang, X., He, X., Fu, X.Y., and Chang, Z. (2006). Varp is a Rab21 guanine nucleotide exchange factor and regulates endosome dynamics. J Cell Sci *119*, 1053-1062.

FIGURE LEGENDS

Figure 1. VAMP7 localizes to melanosomes and is required for pigmentation and cargo trafficking (*a-c*) WT melan-Ink4a melanocytes transiently expressing GFP-VAMP7 (green) were fixed and labeled for TYRP1 (red) and analyzed by deconvolution IFM. Bright field (Melanin) image in *c* is pseudocolored blue in insets. Insets are 5× magnification of the boxed regions. Bar, 10 μm. (*d*) Ultrathin cryosection of transfected WT melan-a melanocytes for EGFP-VAMP7. Arrows indicate VAMP7 at limiting membrane of stage IV melanosomes (IV) and adjacent vesicles. (*e-k*) MNT-1 cells were treated with control siRNA (siCTRL) or VAMP7-specific siRNA (siVAMP7) and analyzed 5d later. (*e*) Whole cell lysates were fractionated by SDS-PAGE and immunoblotted with antibodies to VAMP7 or the AP-1 subunit γ-adaptin as a control. Shown are the regions of the gels encompassing the relevant bands and the positions of nearby molecular weight markers. (*f-g*) Thin sections of fixed cells embedded in epon were analyzed by conventional EM. (*h*) Melanin content in cell lysates was assayed spectrophotometrically. Data are normalized to siCTRL sample and represent mean ± SD from at least three experiments. (*i-j*) Ultrathin cryosections of fixed cells were immunogold labeled for the melanosomal protein TYRP1. Asterisks indicate pigmented melanosomes; arrowheads, TYRP1 labeling on melanosomal membrane or closely adjacent vesicular structures. (*k*) Quantification of TYRP1 localization in control and VAMP7 siRNA treated cells (mean ± SD from three measurements). Vac Endo, vacuolar endosomes; TVE endo, tubulovesicular endosomes associated with endosomes; MVBs, multivesicular bodies; Melano, melanosomes; TVE Melano, tubulovesicular endosomes associated with melanosomes; Lyso, lysosomes; Vesicle,

other vesicular structures; Golgi TGN, Golgi and trans-Golgi network. n.s., no significant difference; *, p<0.05; **, p<0.01; ***, p<0.005. Bars (*f*, *g*, *i*, *j*), 500 nm.

Figure 2. VAMP7 is a BLOC-1 cargo. (*a-j*) BLOC-1-deficient melan-pa (BLOC-$1^{-/-}$) (*a-e*) or "rescued" melan-pa melanocytes stably expressing myc-Pallidin (BLOC-1^{R}) (*f-j*) and transiently expressing GFP-VAMP7 (VAMP7; green) and mCh-STX13 (STX13; red) were fixed and labeled for TYRP1 (cyan) and analyzed by deconvolution IFM. Bright field (BF) images in *d, i* are pseudocolored blue in merge. Arrowheads, GFP-VAMP7 and TYRP1 retained in mCh-STX13-positive endosomes; arrows, melanosomes with GFP-VAMP7 and TYRP1 but lacking mCh-STX13. Insets, 5× magnification of the boxed regions. Bar, 10 μm. (*k-n*) BLOC-$1^{-/-}$ melan-pa melanocytes transiently transfected with GFP-VAMP7 (VAMP7, green), mCh-STX13 (STX13, red) and either myc-Pallidin ("rescue") or myc-Muted ("mock rescue") for indicated times. Bright field images are pseudocolored blue in merge panels. Arrowheads, GFP-VAMP7 retained in mCh-STX13 endosomes; arrows, GFP-VAMP7 labeled melanosomal precursors. Note that pigmentation is not observable until ~72 h following transfection with myc-Pallidin. Insets, 3.5× magnification of the boxed regions. Bar, 10 μM. (*o*) Quantification (mean ± SD) of GFP-VAMP7-labeled structures that lack mCh-STX13 in rescue and mock rescue (Neg. ctl.) cells at 12, 24 and 48 h following transfection. At each time point,15 regions from at least 9 cells representing 3 independent experiments were used for quantification. (*p*) Area (mean ± SD) of overlap between GFP-VAMP7 and mCh-STX13 in the periphery of control and rescue cells quantified at 12, 24 and 48 h following

transfection. For each time point, at least 15 cells representing 4 independent experiments were used for quantification. **, $p < 0.01$; ****, $p < 0.0001$.

Figure 3. VAMP7 and TYRP1 traffic to melanosomes in BLOC-1-dependent membrane tubules. (*a-f*) WT melan-Ink4a melanocytes transiently transfected with mCh-STX13 (STX13, red) and either TYRP1-GFP (TYRP1, green; *a-c*; cell shown in **Fig. S3a**) or GFP-VAMP7 (VAMP7, green; *d-f*; taken from cell shown in **Figures 4d** and **S3b**) and analyzed 24 h later by spinning-disk confocal microscopy at 1 fps. Regions from a single frame are shown. Arrows, mCh-STX13-labeled endosomal tubules; arrowheads, TYRP1-GFP-labeled melanosome (*a-c*) or GFP-VAMP7-labeled tubule (*d-f*). Bar, 1 μm. Note the tubular structure of mCh-STX13-labeled endosomes observed by live cell imaging compared to the punctate pattern observed upon fixation (**Figure 2g, m, n** and elsewhere). (*g-n*) melan-pa melanocytes were transiently transfected with myc-Pallidin, mCh-STX13 and either GFP-VAMP7 (*g-j*) or TYRP1-GFP (*k-n*) and analyzed 18 h later by spinning-disk confocal microscopy at ~1 fps. (*g* and *k*) Single frames of representative cells showing overlap of mCh-STX13 with GFP-VAMP7 (*g*) or TYRP1-GFP (*k*). Bars, 10 μm. Image sequences from the boxed region in *g* and *k* are shown magnified 5× in *h-j* and *l-n*, respectively. Arrows, mCh-STX13-labeled tubules containing GFP-VAMP7 (*h-j*) or TYRP1-GFP (*l-n*). Elapsed time (sec) is indicated in seconds at lower right; bar, 1 μm.

Figure 4. GFP-VAMP7 exits melanosomes in STX13-independent tubules lacking TYRP1. (*a-f*) WT melan-Ink4a melanocytes transiently transfected with GFP-VAMP7

alone (green, *a-c*) or with mCh-STX13 (red, *d-g*) or TYRP1-mRFP (red, *h-j*) and analyzed 24 h later by spinning-disk confocal microscopy at ~1 fps. (*a-c*) Image sequence from a cell (shown in **Figure S4a**) expressing GFP-VAMP7 relative to melanosomes visualized by bright field microscopy (BF). Arrow, GFP-VAMP7 tubule; arrowhead, melanosome in bright field image. Bar, 2 μm. (*d*) Single frame from representative cell expressing GFP-VAMP7 and mCh-STX13. Bar, 10 μm. (*e-g*) Single frames from regions indicated in *d* with single channels and merged image. Arrows, tubules labeled by GFP-VAMP7 (VAMP7, green); arrowheads, tubules labeled by mCh-STX13 (STX13, red). Bar, 1 μm. Insets are magnified 2× from *d*. (*h-j*) Image sequence from a cell (shown in **Figure S4b**) expressing GFP-VAMP7 (VAMP7, green) and TYRP1-mRFP (TYRP1, red). A GFP-VAMP7-labeled tubule (arrow) emerges from a TYRP1-mRFP/GFP-VAMP7-labeled melanosome (arrowhead). Bar, 2 μm.

Figure 5. VARP localizes to melanosomes and is present on departing GFP-VAMP7-containing tubules. (*a-i*) WT melan-Ink4a melanocytes transiently transfected with VARP-GFP and mCh-VAMP7 (*a-c*), GFP-VAMP7 and VARP-HA (*d-f*) or VARP-GFP and mCh-STX13 (*g-i*) were fixed 48 h following transfection, labeled with anti-HA (*d-f*), and analyzed by deconvolution IFM. Bright field images are pseudocolored blue and shown in merge and insets. Insets, 5× magnification of boxes. (*a-f*) Arrowheads, VARP puncta adjacent to melanosomes (*a-f*) or to mCh-STX13-labeled endosomes (*g-i*). Bar, 10 μm. (*j-u*) WT melan-Ink4a melanocytes transiently transfected with VARP-GFP and either mCh-VAMP7 (*j-l*; see **Figure S5a**), OCA2-mRFP (*m-o*; see **Figure S5b**) or mCh-STX13 (*p-u*; see **Figure S5c**, **d**) and analyzed 48 h later by spinning-disk confocal

microscopy at 1 fps. Elapsed time (in sec) is indicated at lower right. Bar, 2 μm. (*j*-*l*) A VARP-GFP- and mCh-VAMP7-labeled tubule (arrow) extends from a melanosome (arrowhead). (*m*-*o*) A VARP-GFP-labeled vesicle (arrow) exits from an OCA2-mRFP-labeled melanosome (arrowhead). (*p*-*r*) A VARP-GFP tubule (arrow) departs from a mCh-STX13-labeled endosome (arrowhead). (*s*-*u*) A mCh-STX13 tubule (arrow) exits from a mCh-STX13/VARP-GFP-double labeled endosome (arrowhead). Bars, 2 μm.

Figure 6. VARP is localized to melanosomes by interaction with both VAMP7 and RAB38. (*a*-*m*) WT melan-Ink4a melanocytes transiently transfected with GFP-RAB38 (green) and either VARP-HA (red, *a*-*d*), or mCh-VAMP7 (red, *e*-*h*) or with mCh-STX13 (STX13, red) and either WT VARP-GFP (green, *i*) or site-directed mutants (green, *j*-*m*) with interfering mutations in the binding sites for VAMP7 (-VAMP7, *j*), RAB38 (-RAB38, *k*), both VAMP7 and RAB38 (-V7, RAB38, *l*) or the VPS29 retromer subunit (-retromer, *m*). Cells were fixed 48 h following transfection, labeled with anti-HA (*a*-*d*), and analyzed by deconvolution IFM. Bright field (BF) images are pseudocolored blue and shown in merge and insets. Insets, 5× magnification of boxed regions. Bar, 10 μm. (*a*-*d*) Arrowheads, VARP-HA and GFP-RAB38 puncta adjacent to melanosomes. (*e*-*h*) Arrowheads, GFP-RAB38 and mCh-VAMP7 localized to melanosomes. (*i*-*m*) Arrowheads, VARP-GFP puncta adjacent to melanosomes visualized by bright field; arrows, VARP-GFP puncta adjacent to mCh-STX13-labeled endosomes. Bar, 10 μm. (*n*) Puncta labeled by VARP-GFP WT or mutants that were associated with melanosomes (visualized by bright field; black bars) or with endosomes (labeled by mCh-STX13; gray bars) were quantified as mean ± SD. (*o*) p-values for melanosome-

associated VARP puncta in *p*. For each VARP-GFP mutant, 10 cells representing 3 independent experiments were analyzed. For endosome-associated VARP, only -V7 & R38 ($p<0.05$ vs. WT) and -retromer ($p<0.0001$ vs. all others) showed significant differences.

Figure 7. BLOC-3 is required to generate VAMP7/VARP-containing recycling tubules. (*a*-*r*) HPS4-deficient melan-le (le) and melan-le cells stably expressing HA-HPS4 (le:HPS4) were transiently transfected with mCh-VAMP7 (red, VAMP7) and either GFP-RAB38 (green, RAB38, *a*-*j*), or VARP-GFP (green, VARP, *k*-*r*), fixed 24 h (*a*-*j*) or 48 h (*k*-*r*) following transfection, labeled for TYRP1 (cyan, *a*-*j*), and analyzed by deconvolution IFM. Bright field (BF) images are pseudocolored blue and shown in merge and insets in *a*-*j* together with RAB38 and VAMP7. Insets, 5× magnifications of boxes. Bar, 10 μm. (*a*-*j*) Arrows, mCh-VAMP7 and TYRP1 colocalized to melanosomes visualized by bright field. Note RAB38-GFP localization to melanosomes in le:HPS4 (*f*) but not in le (*a*). (*k*-*r*) Large arrowhead in le main panel shows perinuclear accumulation of VARP-GFP. Small arrowheads in insets, VARP-GFP puncta associated with melanosomes; arrows, melanosomes lacking VARP-GFP puncta. (*s*-*u*) WT melan-Ink4a, melan-le, melan-le:HPS1 or melan-le:HPS4 cells were transiently transfected with GFP-VAMP7 and analyzed by spinning-disk confocal microscopy 24 h later. Images were acquired at ~1 fps and a segment of the image sequence is shown. Elapsed time (in sec) is indicated at lower right; bar, 2 μm. Arrows, GFP-VAMP7 tubules or vesicles leaving GFP-VAMP7-labeled melanosomes. (*v*) Fission of GFP-VAMP7 transport intermediates from melanosomes was quantified by counting events within 26.5 μm^2

regions in the cell periphery during 5 min image sequences acquired at 1 fps. At least 15 regions from a minimum of 6 cells, representing 3 independent experiments, were quantified for each cell type. ****, $p < 0.0001$.

Figure 1.

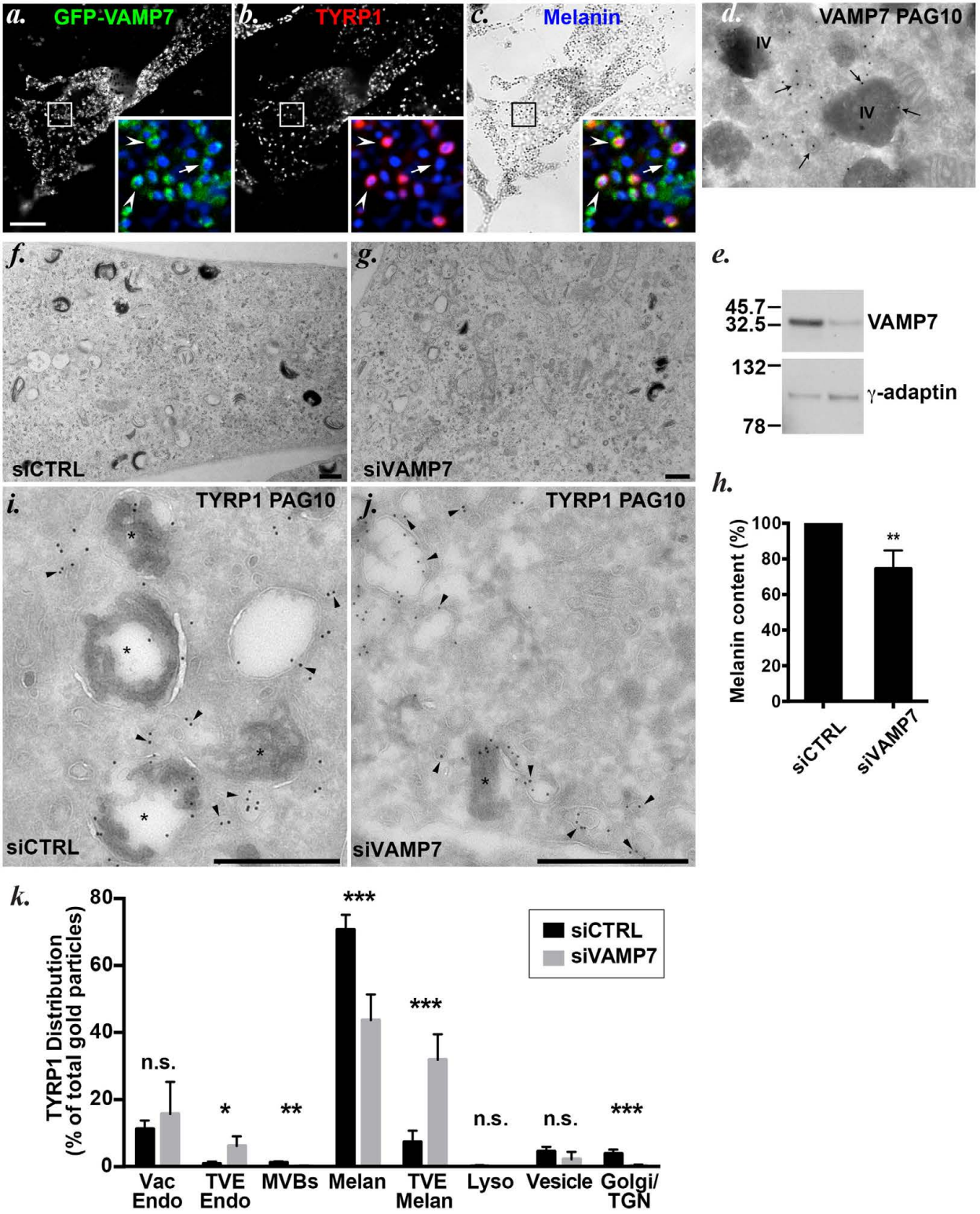
a.
GFP-VAMP7
b.
TYRP1
c.
Melanin
d.
VAMP7 PAG10
IV
IV
f.
siCTRL
g.
siVAMP7
e.
45.7
32.5
VAMP7
132
γ-adaptin
78
h.
Melanin content (%)
100
80
60
40
20
0
**
siCTRL
siVAMP7
i.
TYRP1 PAG10
siCTRL
j.
TYRP1 PAG10
siVAMP7
k.
TYRP1 Distribution
(% of total gold particles)
80
60
40
20
0
siCTRL
siVAMP7
n.s.
*
**
***
***
n.s.
n.s.
***
Vac Endo
TVE Endo
MVBs
Melan
TVE Melan
Lyso
Vesicle
Golgi/ TGN

Figure 2.

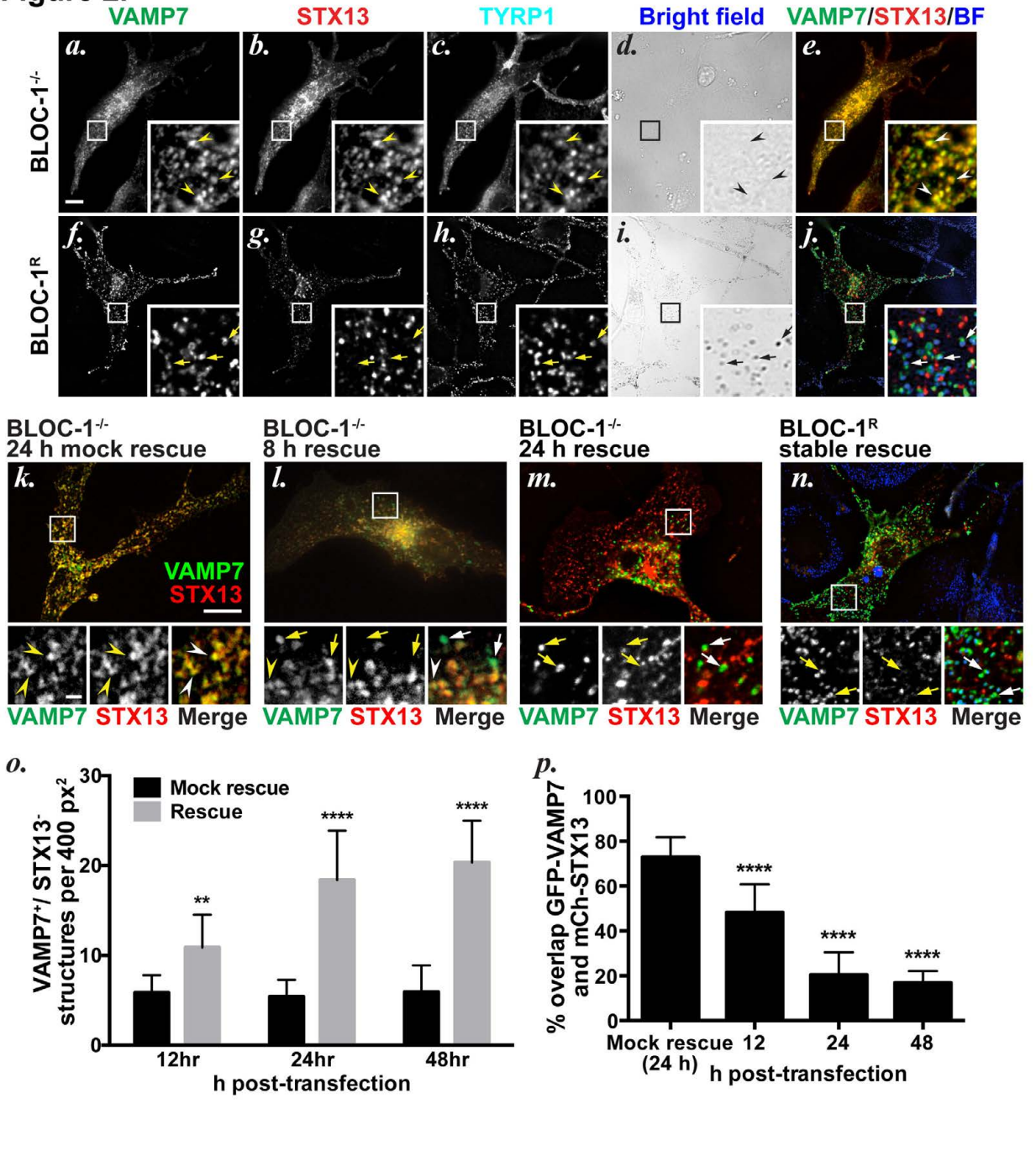
VAMP7
STX13
TYRP1
Bright field
VAMP7/STX13/BF
BLOC-1-/-
BLOC-1R
a.
b.
c.
d.
e.
f.
g.
h.
i.
j.
BLOC-1-/-
24 h mock rescue
BLOC-1-/-
8 h rescue
BLOC-1-/-
24 h rescue
BLOC-1R
stable rescue
k.
l.
m.
n.
VAMP7
STX13
VAMP7 STX13 Merge
VAMP7 STX13 Merge
VAMP7 STX13 Merge
VAMP7 STX13 Merge
o.
VAMP7+/ STX13- structures per 400 px2
Mock rescue
Rescue
**
****
****
12hr
24hr
48hr
h post-transfection
p.
% overlap GFP-VAMP7 and mCh-STX13
****
****
****
Mock rescue (24 h)
12
24
48
h post-transfection

Figure 3.

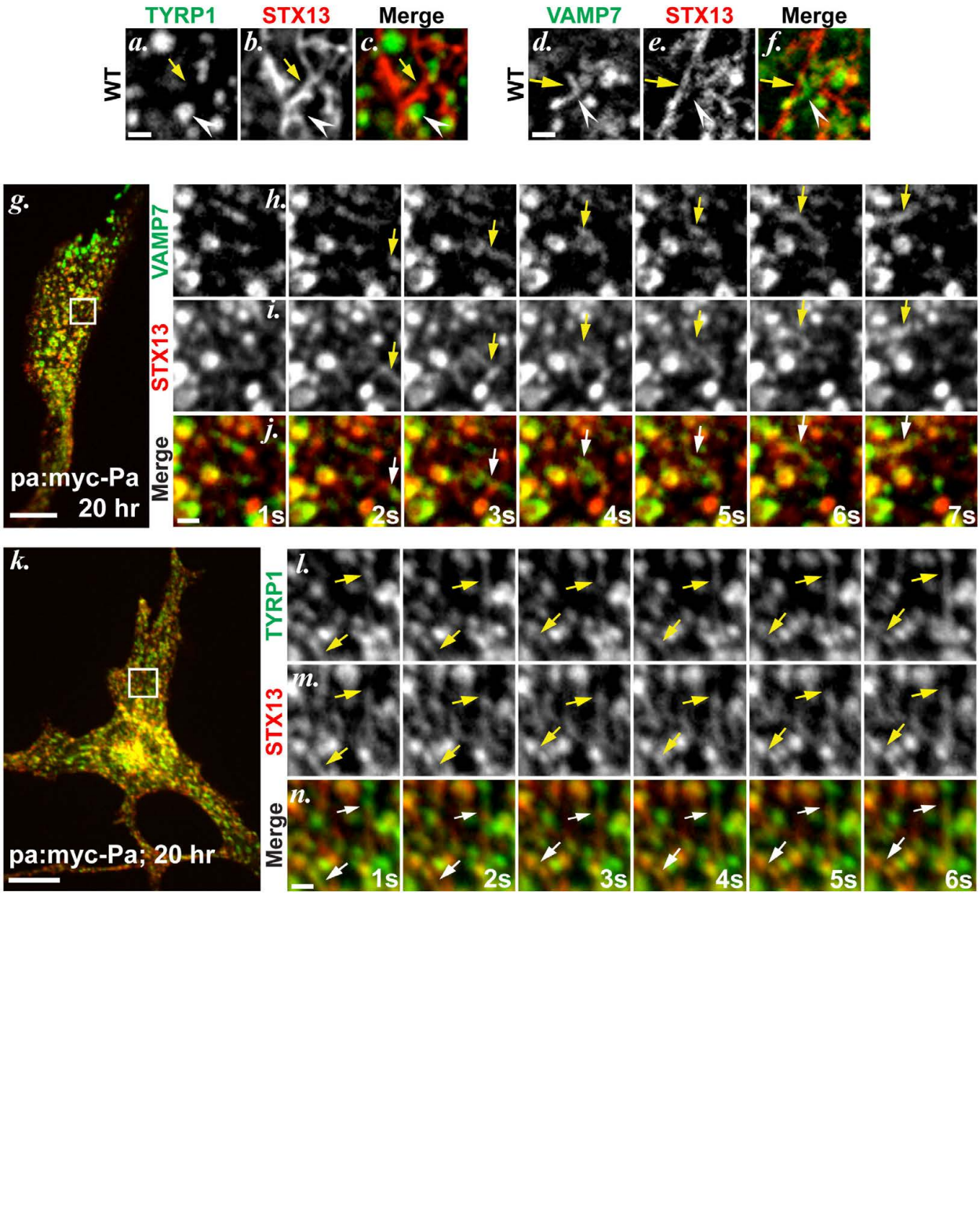
TYRP1
STX13
Merge
VAMP7
STX13
Merge
WT
WT
a.
b.
c.
d.
e.
f.
g.
h.
i.
j.
VAMP7
STX13
Merge
pa:myc-Pa
20 hr
1s
2s
3s
4s
5s
6s
7s
k.
l.
m.
n.
TYRP1
STX13
Merge
pa:myc-Pa; 20 hr
1s
2s
3s
4s
5s
6s

Figure 4.

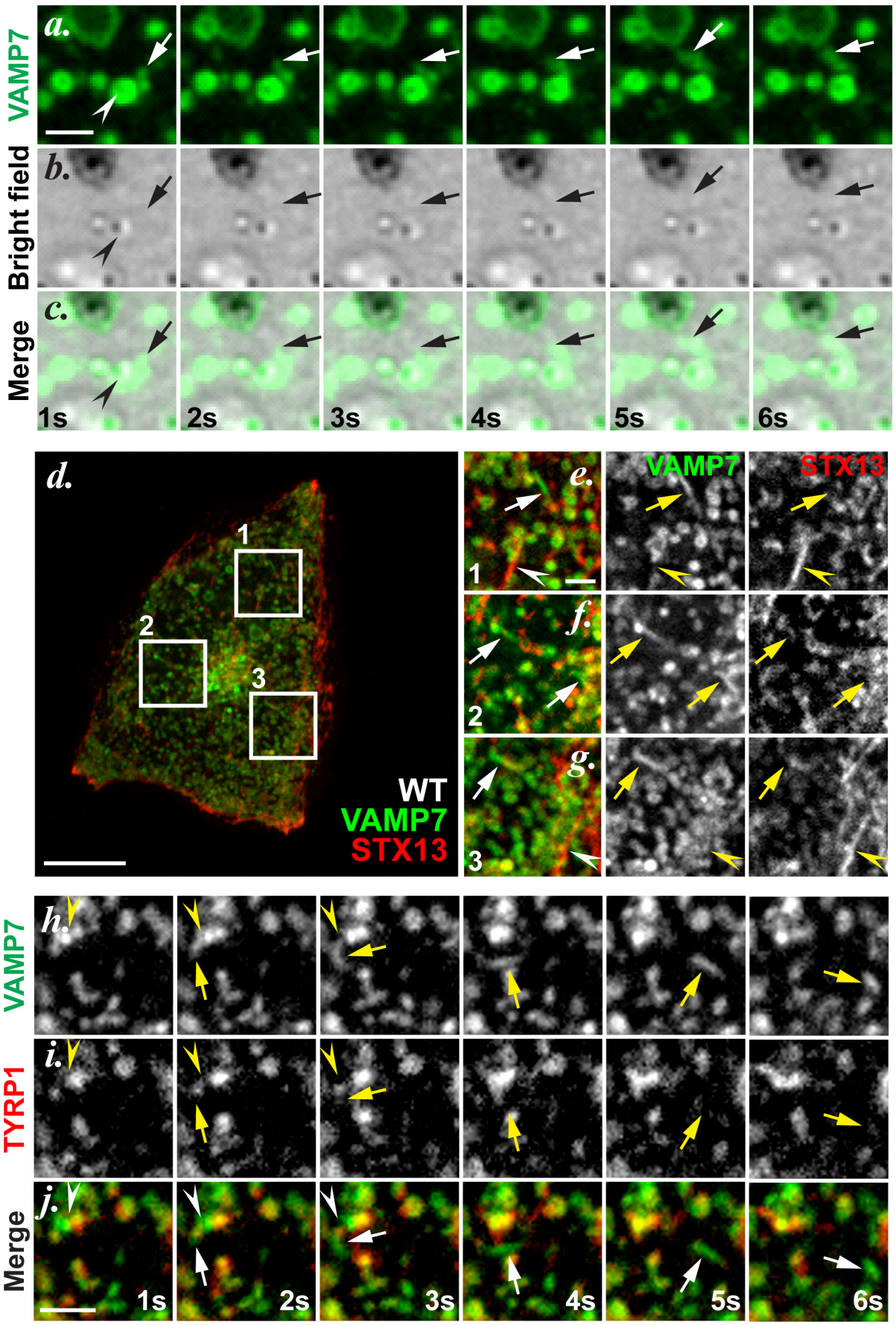
a.
VAMP7
b.
Bright field
c.
Merge
1s
2s
3s
4s
5s
6s
d.
1
2
3
WT
VAMP7
STX13
e.
f.
g.
VAMP7
STX13
h.
VAMP7
i.
TYRP1
j.
Merge
1s
2s
3s
4s
5s
6s

Figure 5.

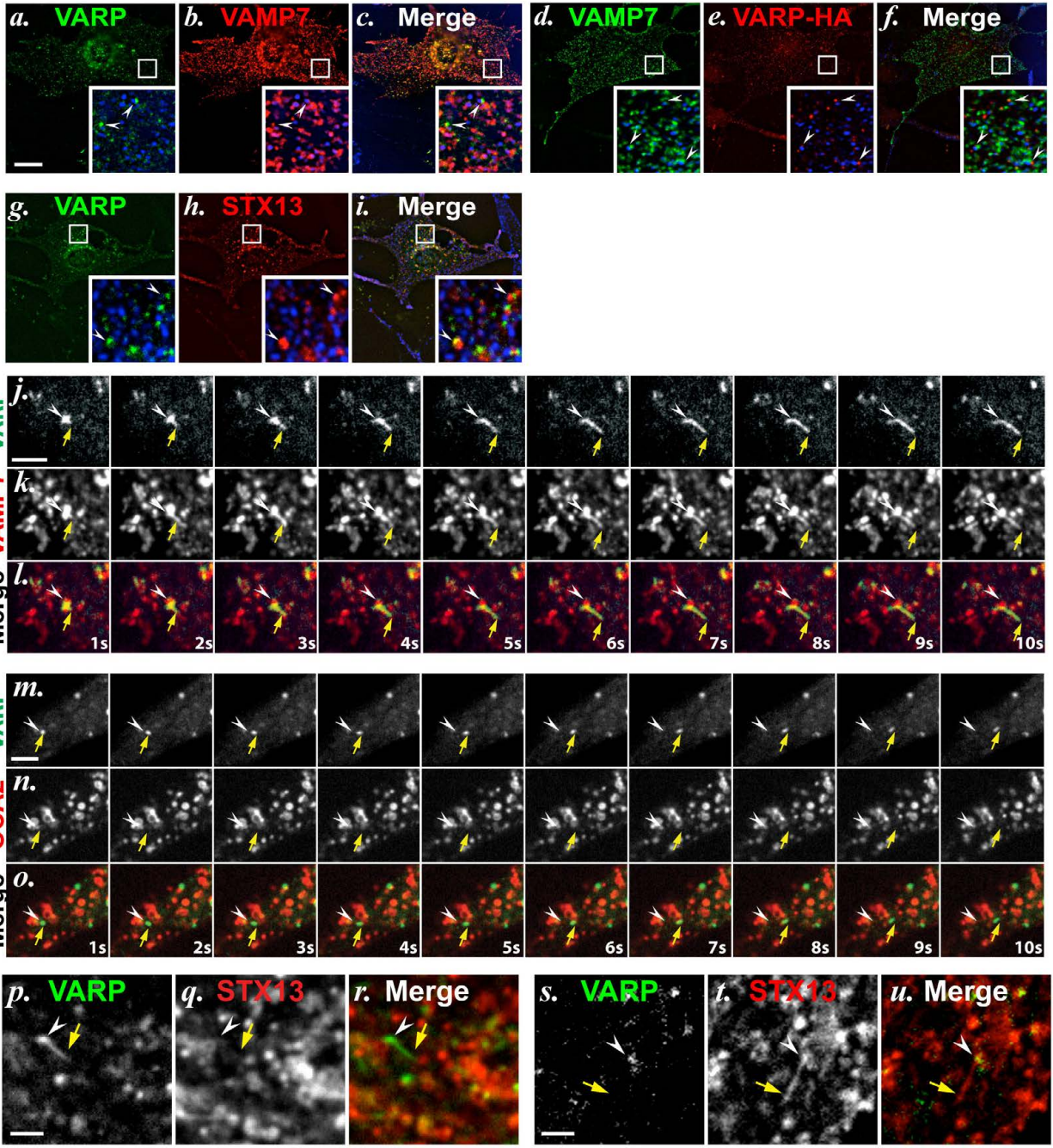
a. VARP
b. VAMP7
c. Merge
d. VAMP7
e. VARP-HA
f. Merge
g. VARP
h. STX13
i. Merge
j.
VARP
k.
VAMP7
l.
Merge
1s
2s
3s
4s
5s
6s
7s
8s
9s
10s
m.
VARP
n.
OCA2
o.
Merge
1s
2s
3s
4s
5s
6s
7s
8s
9s
10s
p. VARP
q. STX13
r. Merge
s. VARP
t. STX13
u. Merge

Figure 6.

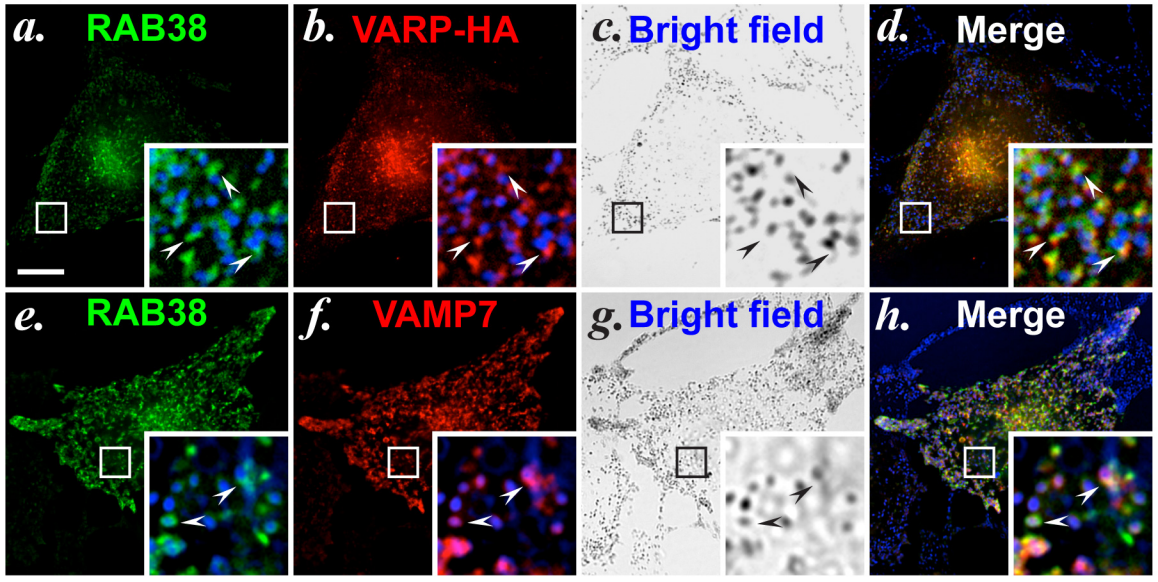

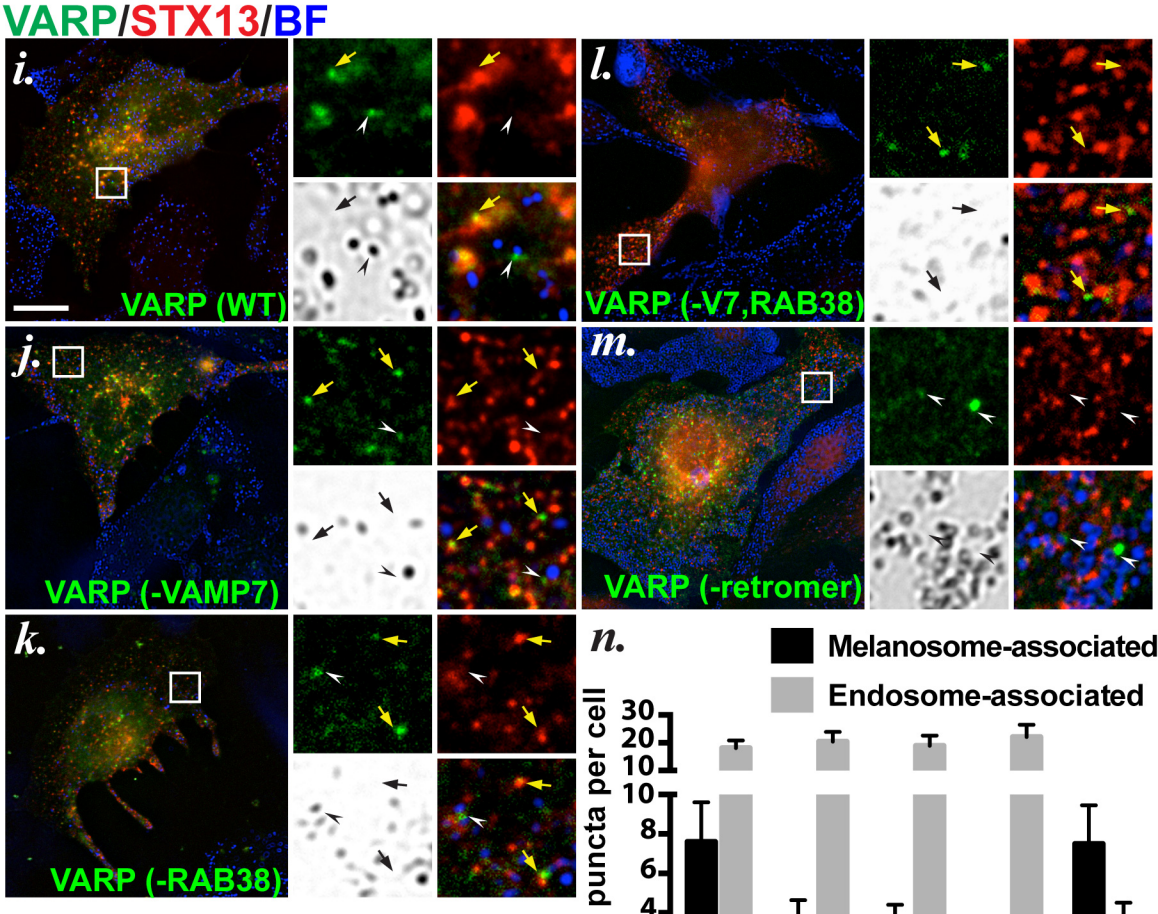

o.

	WT	-VAMP7	-RAB38
-VAMP7	****	—	ns
-RAB38	****	ns	—
-V7 & R38	****	***	***
-retromer	ns	****	****

Figure 7.

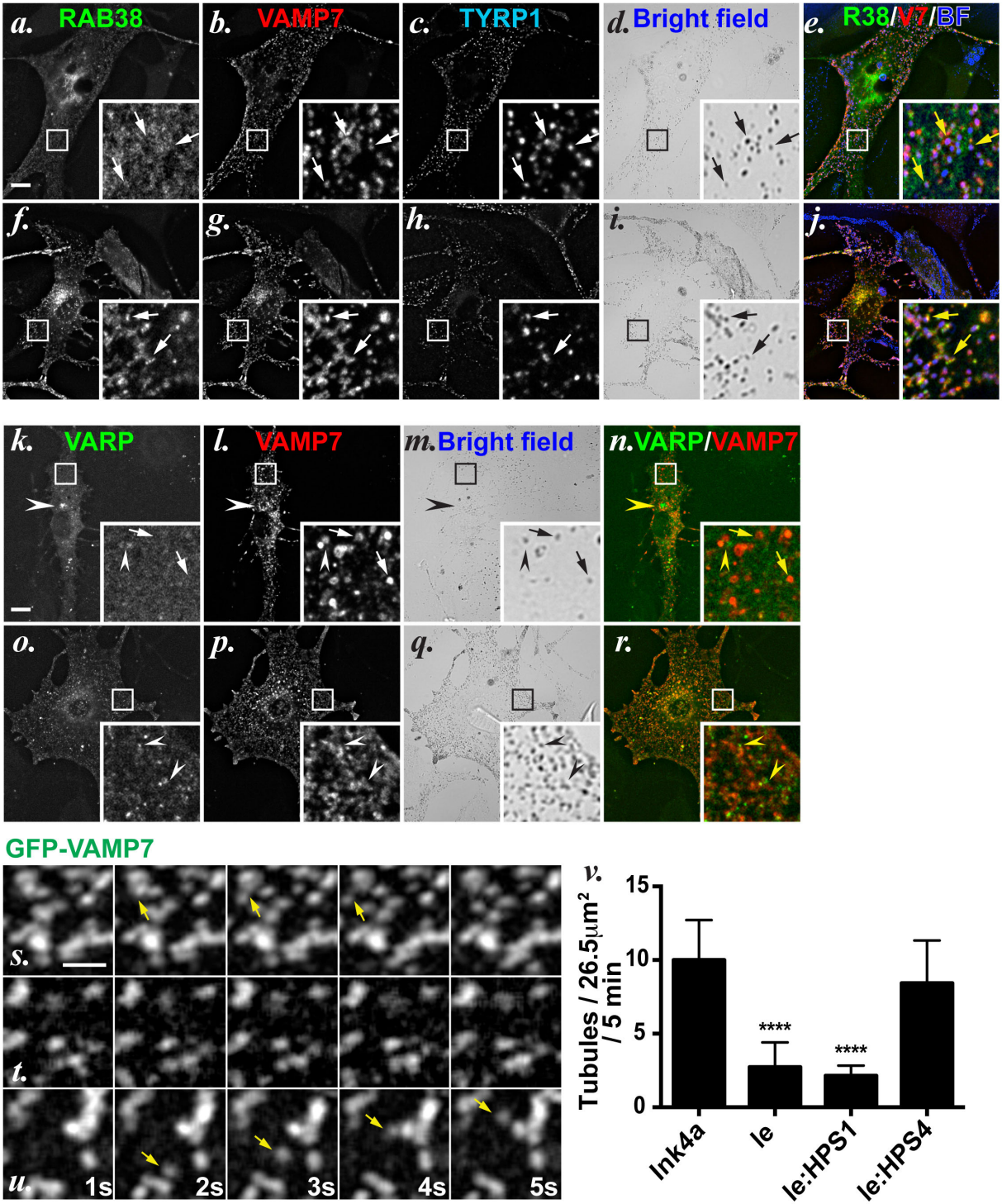
a. RAB38
b. VAMP7
c. TYRP1
d. Bright field
e. R38/V7/BF
le
f.
g.
h.
i.
j.
le:HPS4
k. VARP
l. VAMP7
m. Bright field
n. VARP/VAMP7
le
o.
p.
q.
r.
le:HPS4
GFP-VAMP7
Ink4a
s.
le
t.
le:HPS4
u.
1s
2s
3s
4s
5s
v.
Tubules / 26.5μm² / 5 min
15
10
5
0
****
****
Ink4a
le
le:HPS1
le:HPS4